Transformation of a rolling mill aggregate to a Cyber Physical Production System: from sensor retrofitting to machine learning

Benjamin James Ralph (benjamin.ralph@unileoben.ac.at)
Montanuniversitat Leoben https://orcid.org/0000-0002-3058-7178
Marcel Sorger
Montanuniversitat Leoben
Karin Hartl
Montanuniversitat Leoben
Andreas Schwarz
Montanuniversitat Leoben
Florian Messner
Montanuniversitat Leoben
Martin Stockinger
Montanuniversität Leoben: Montanuniversitat Leoben

Research Article

Keywords: Cyber Physical Production System, Retrofitting, Digitalization, Digital Twin, Machine Learning, Smart Forming Lab, Industry 4.0

Posted Date: March 31st, 2021

DOI: https://doi.org/10.21203/rs.3.rs-355228/v1

Version of Record: A version of this preprint was published at Journal of Intelligent Manufacturing on October 24th, 2021. See the published version at https://doi.org/10.1007/s10845-021-01856-2.

Abstract

This paper describes the transformation of a rolling mill aggregate from a stand-alone solution to a fully integrated cyber physical production system. Within this process, already existing load cells were substituted and additional inductive and magnetic displacement sensors were applied. After calibration, those were fully integrated into a six-layer digitalization architecture at the Smart Forming Lab at the Chair of Metal Forming (Montanuniversitaet Leoben). Within this framework, two front end human machine interfaces were designed, where the first one serves as a condition monitoring system during the rolling process. The second user interface visualizes the result of a resilient machine learning algorithm, which was designed using Python and is not just able to predict and adapt the resulting rolling schedule of a defined metal sheet, but also to learn from additional rolling mill schedules carried out. This algorithm was created on the basis of a black box approach, using data from more than 1900 milling steps with varying roll gap height, sheet width and friction conditions. As a result, the developed program is able to interpolate and extrapolate between these parameters as well as different initial sheet thicknesses, serving as a digital twin for data-based recommendations on schedule changes between different rolling process steps. Furthermore, via the second user interface, it is possible to visualize the influence of this parameters on the result of the milling process. As the whole layer system runs on an internal server at the university, students and other interested parties are able to access the visualization and can therefore use the environment to deepen their knowledge within the characteristics and influence of the sheet metal rolling process as well as data science and especially fundamentals of machine learning. This algorithm also serves as a basis for further integration of materials science based data for the prediction of the influence of different materials on the rolling result. To do so, the rolled specimens were also analyzed regarding the influence of the plastic strain path on their mechanical properties, including anisotropy and materials' strength.

Full Text

This preprint is available for download as a PDF.

Figures

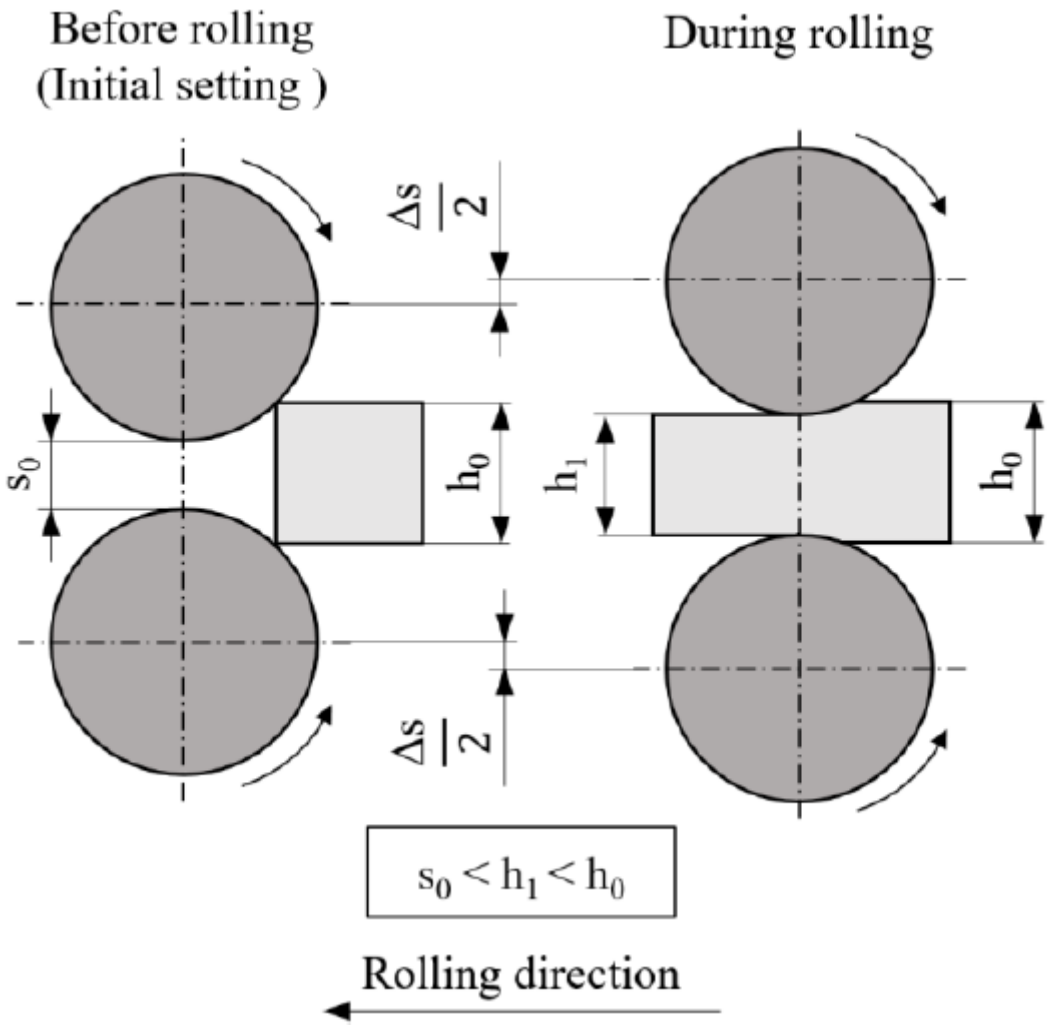

Figure 1

Geometry change during rolling

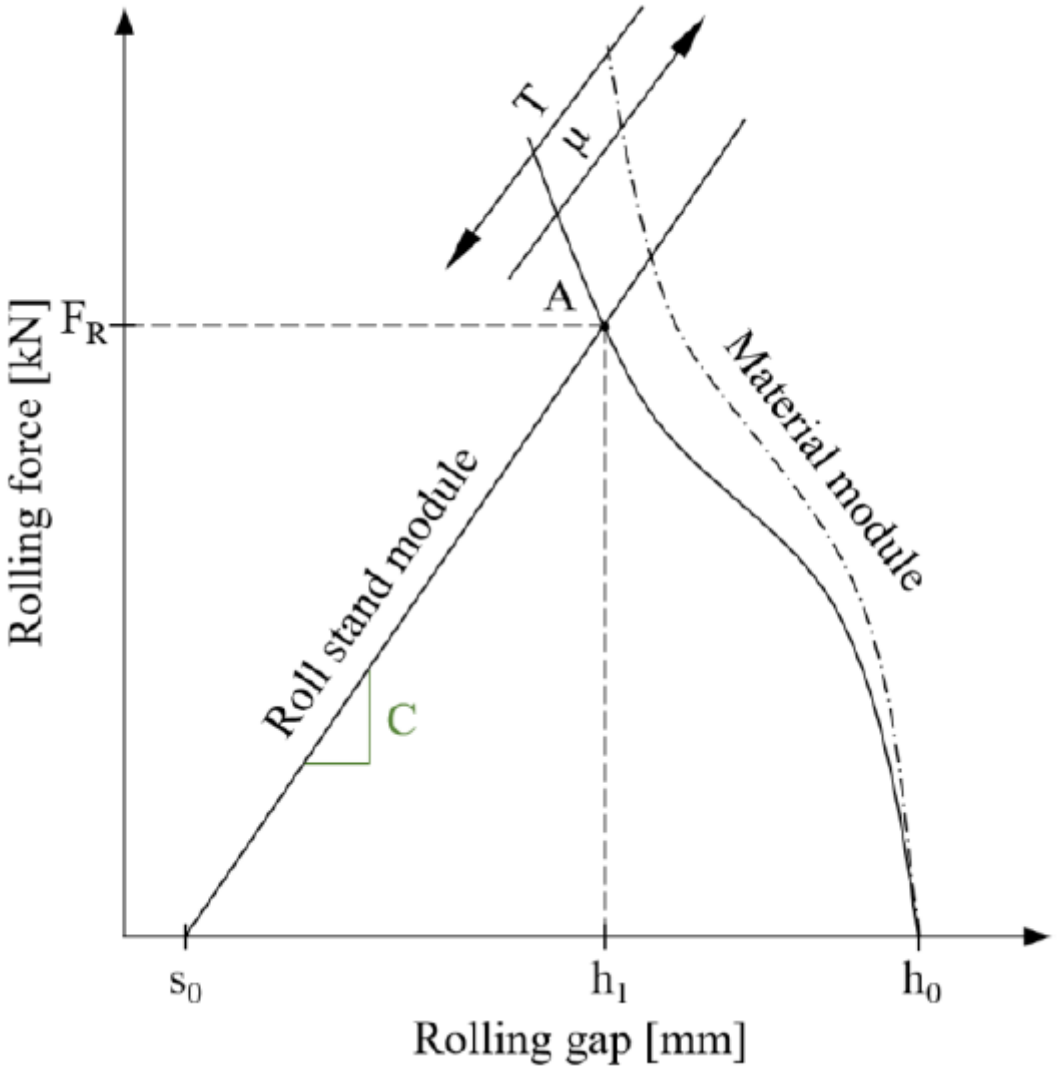

Figure 2

Work diagram for rolling for a defined s0.

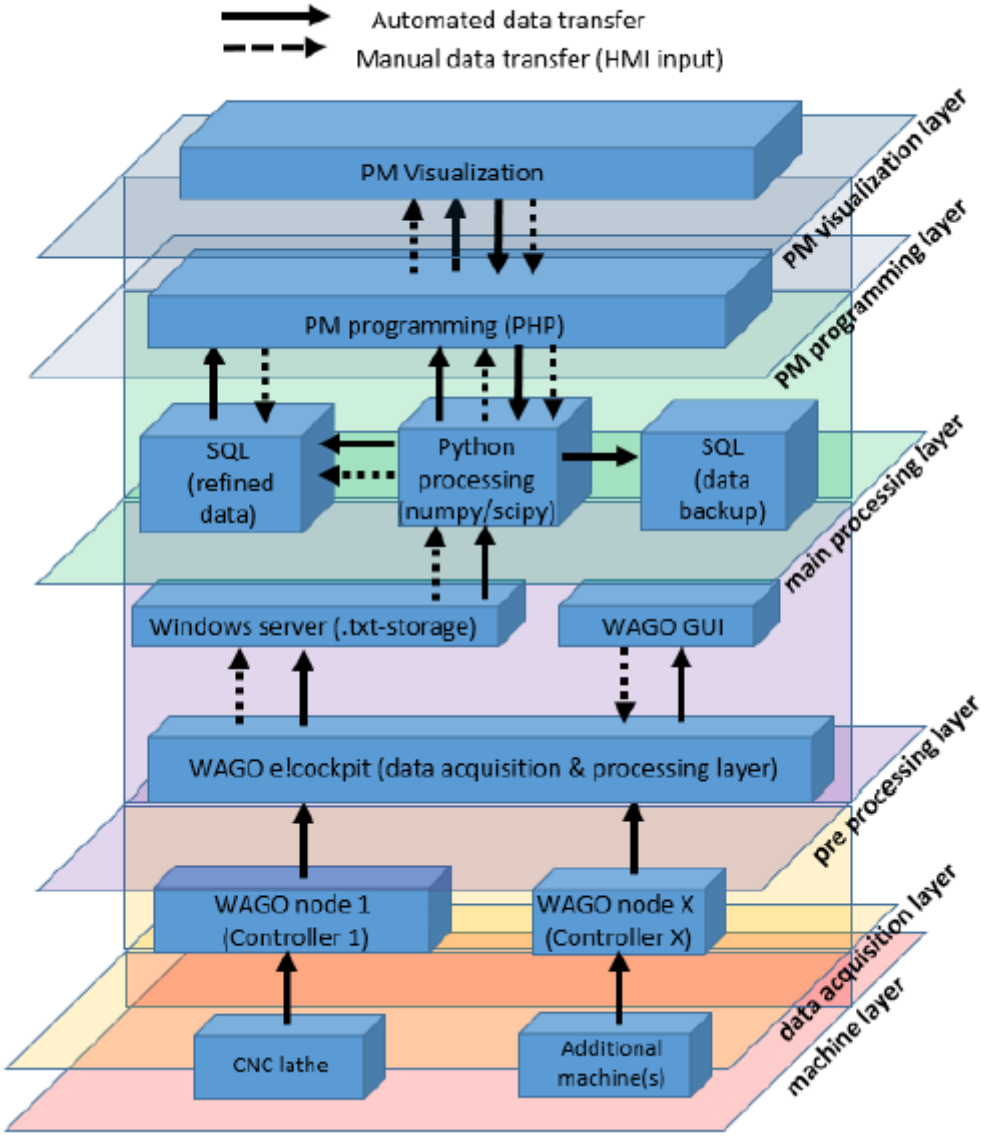

Figure 3

Initial state of the six-layer architecture at the SFL (Ralph, Sorger et al. 2021)

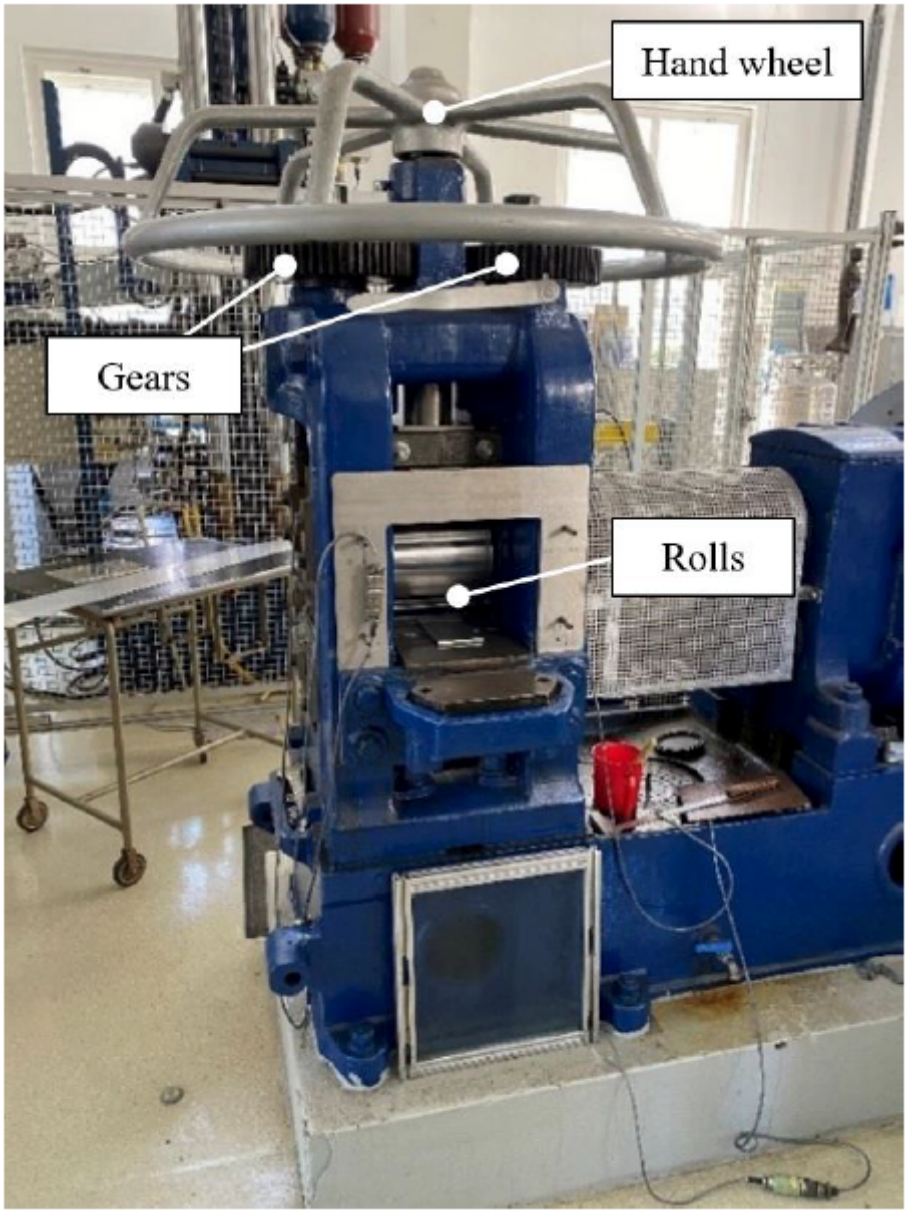

Figure 4

Rolling mill system: initial state

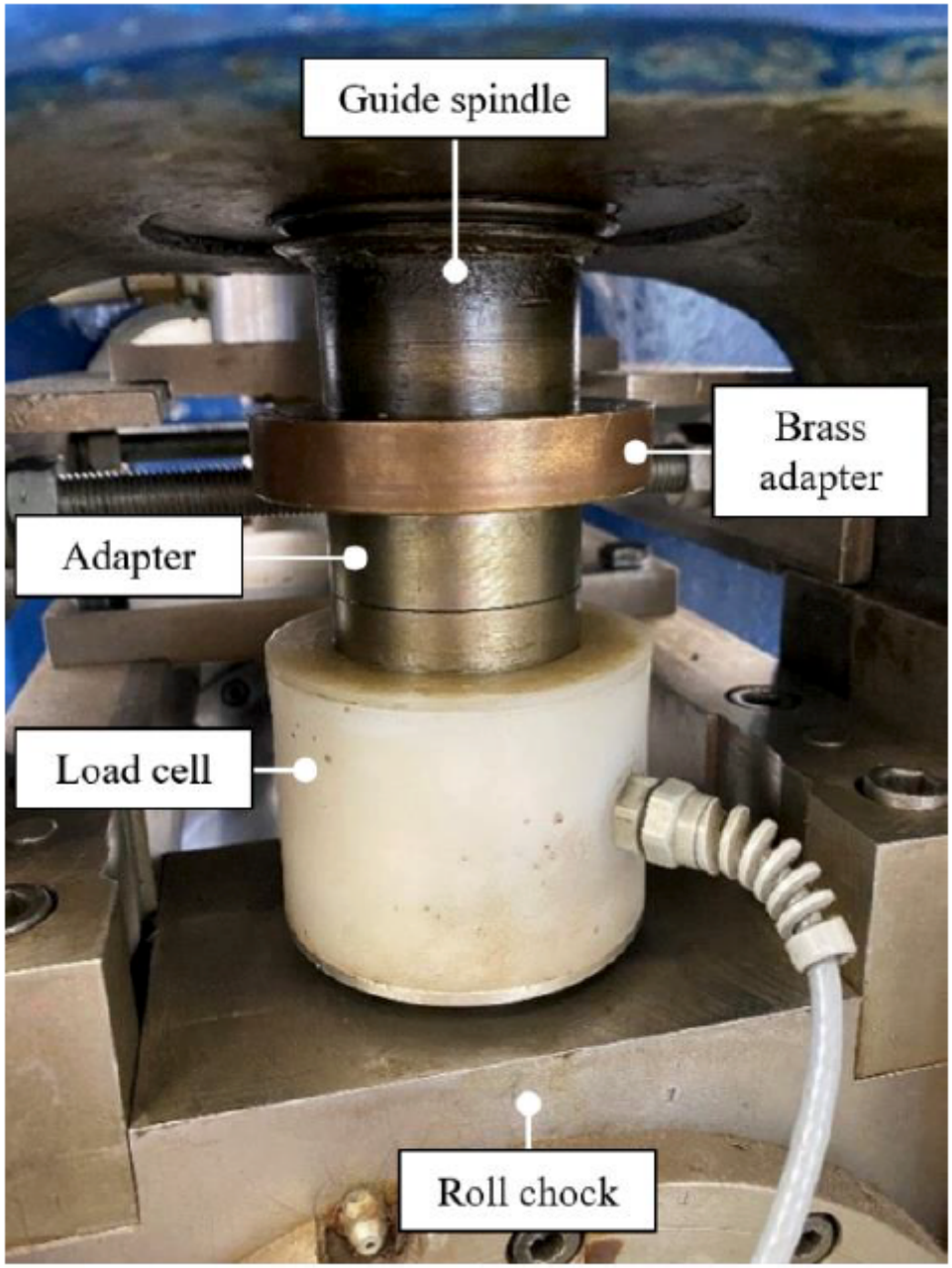

Figure 5

Load cell of the left guide spindle: initial state

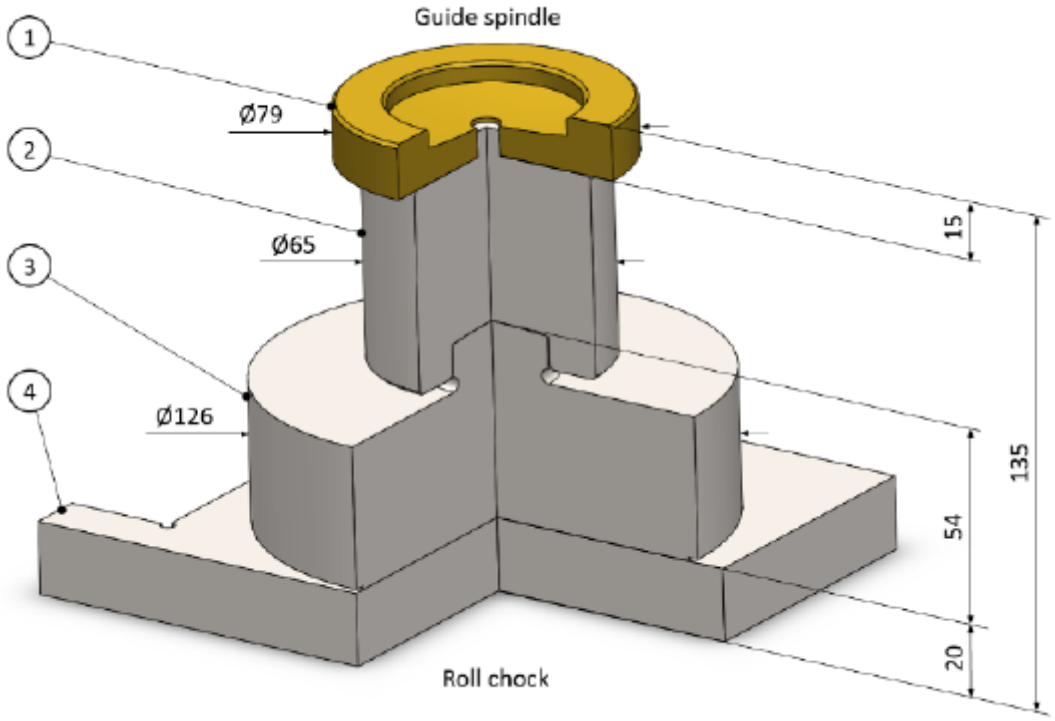

Figure 6

Construction scheme of the new designed load measurement unit

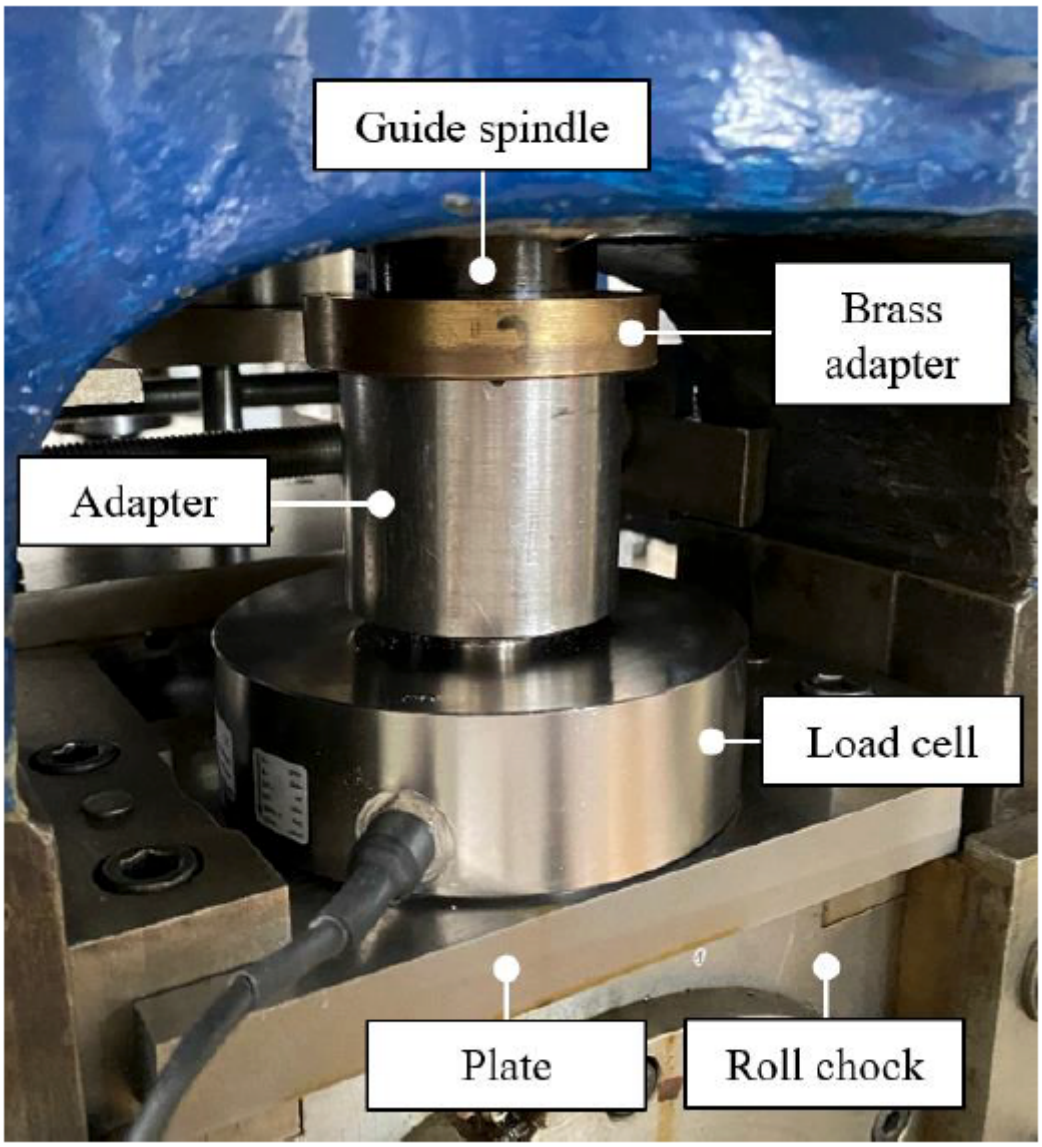

Figure 7

Resulting implementation of the new designed load measurement unit

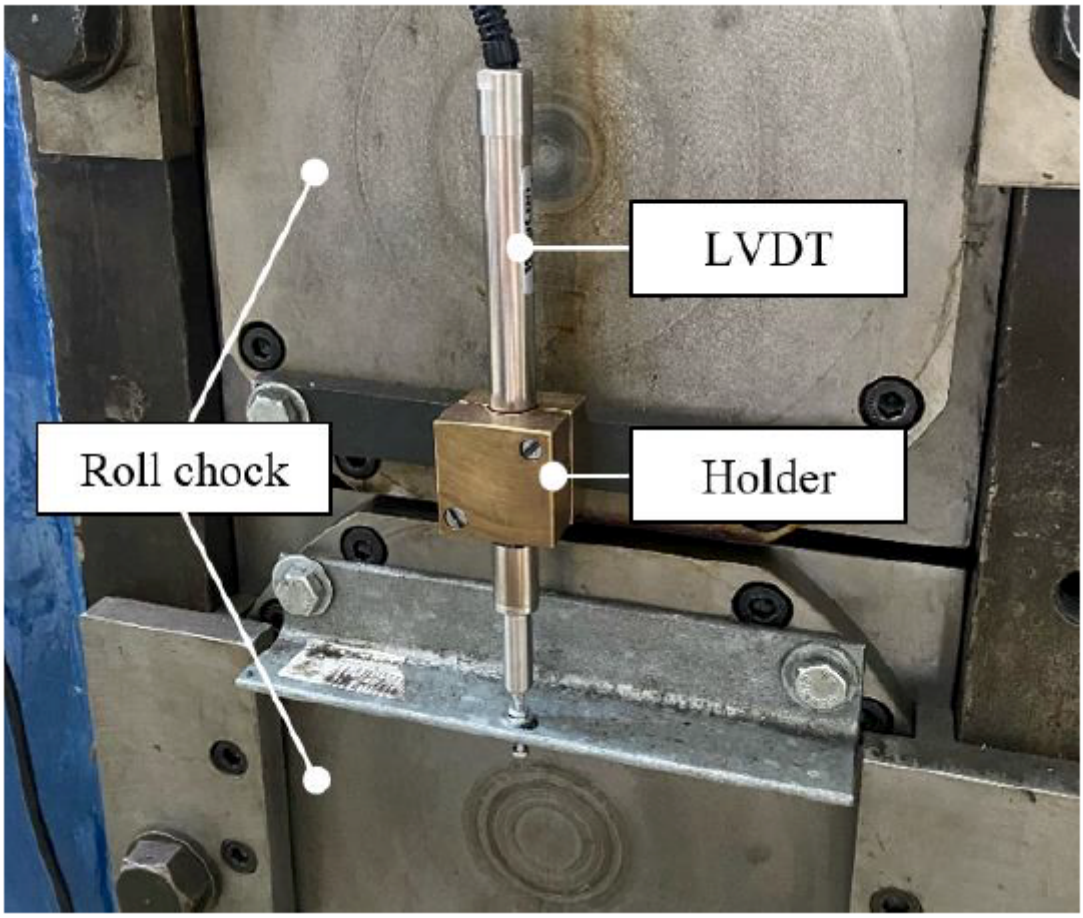

Figure 8

Mounted LVDT sensor

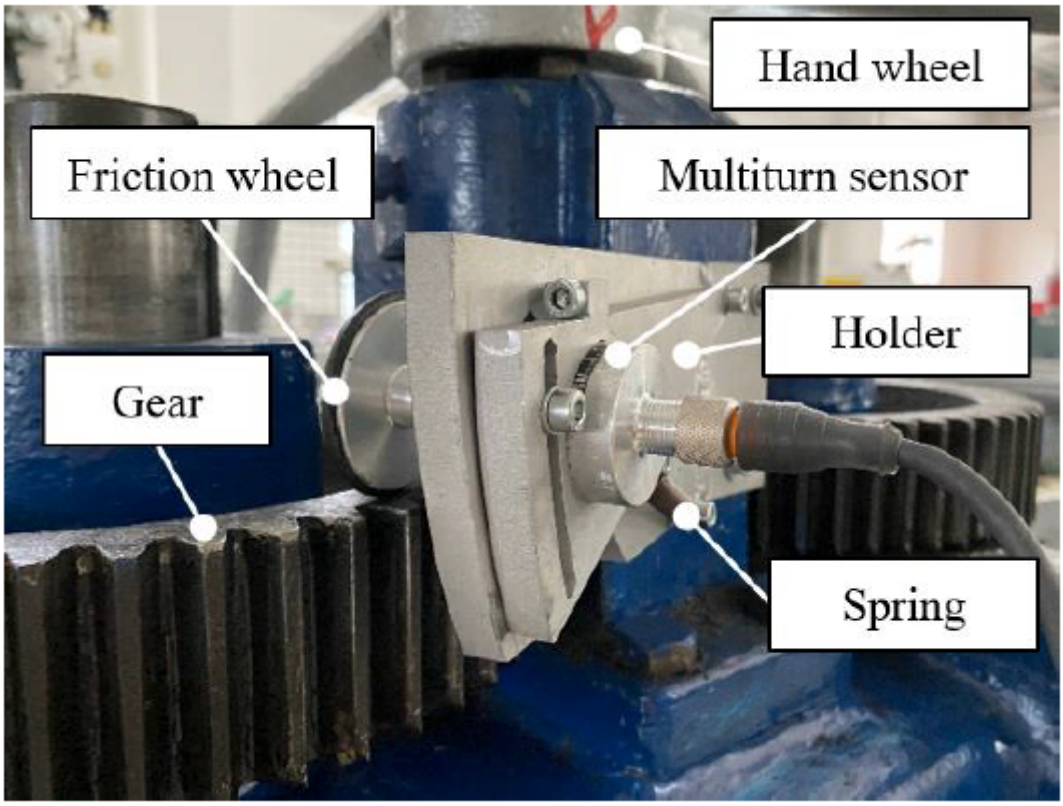

Figure 9

Mounted multiturn encoder

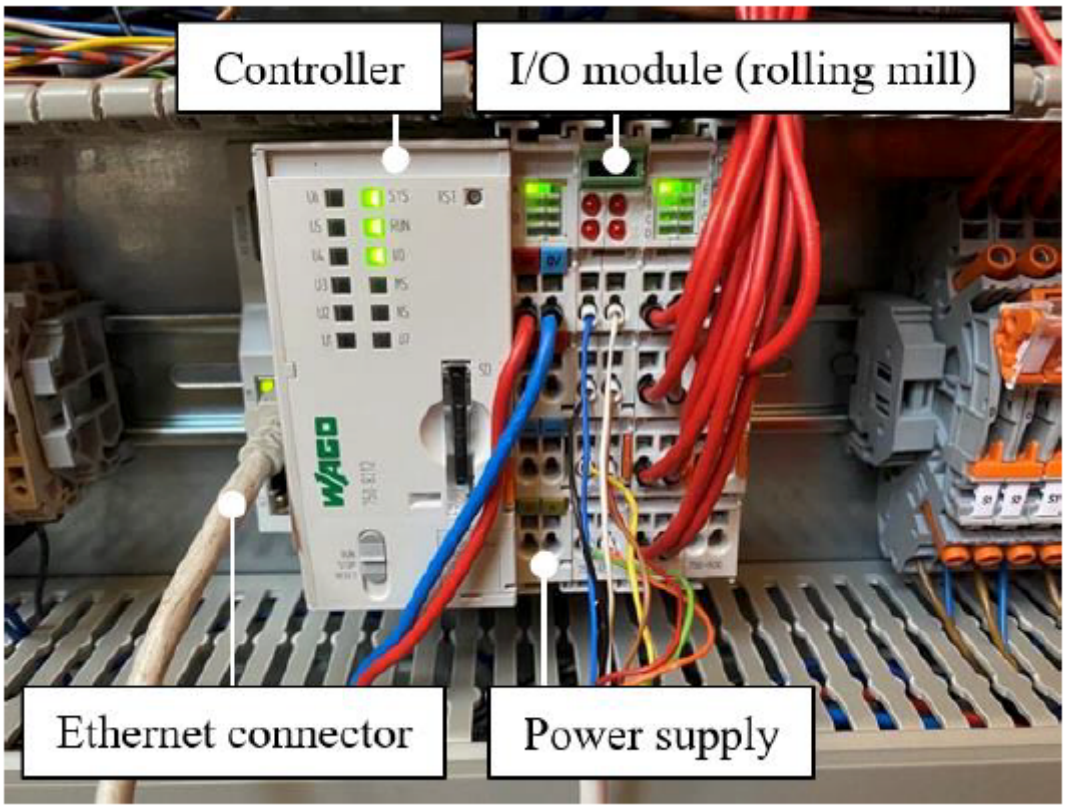

Figure 10

Controller and I/O modules

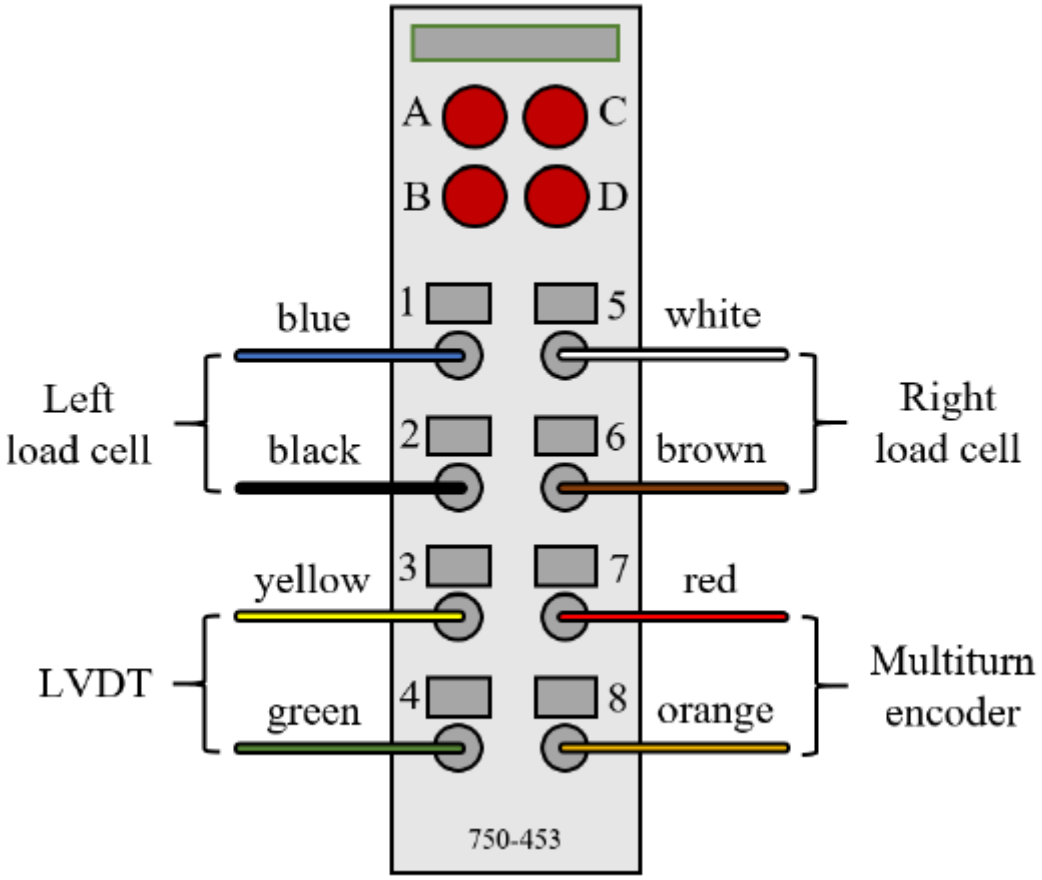

Figure 11

Circuit diagram of the connection rolling mill sensors/DAQ

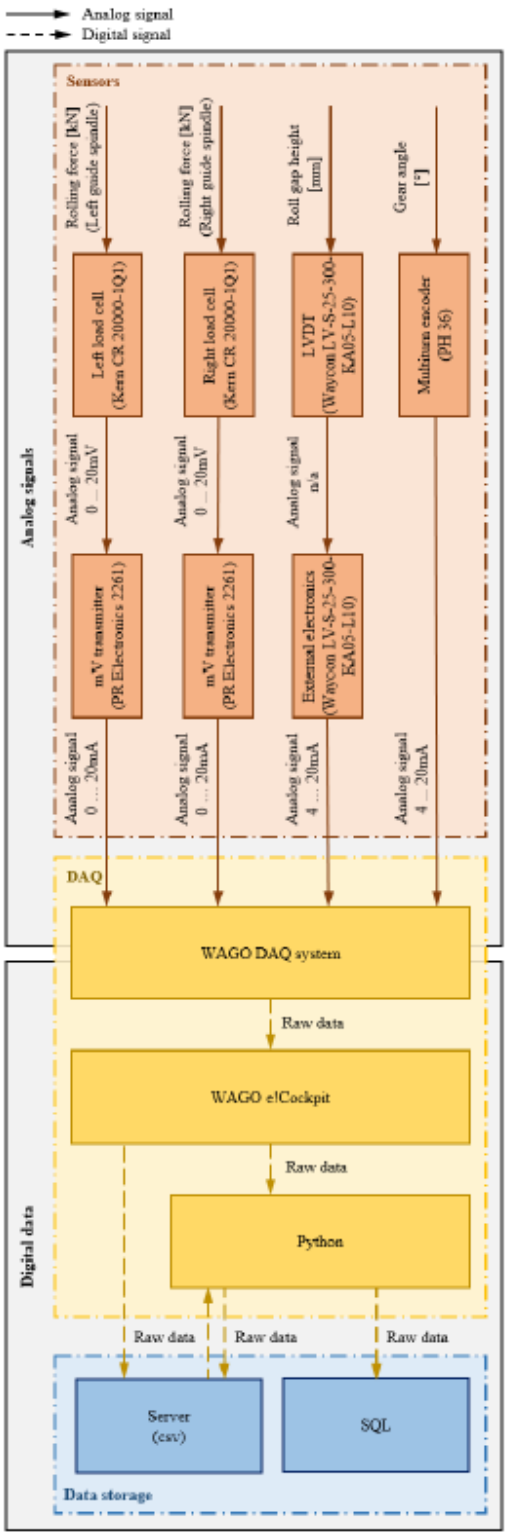

Figure 12

Sensor connection and A/D conversion

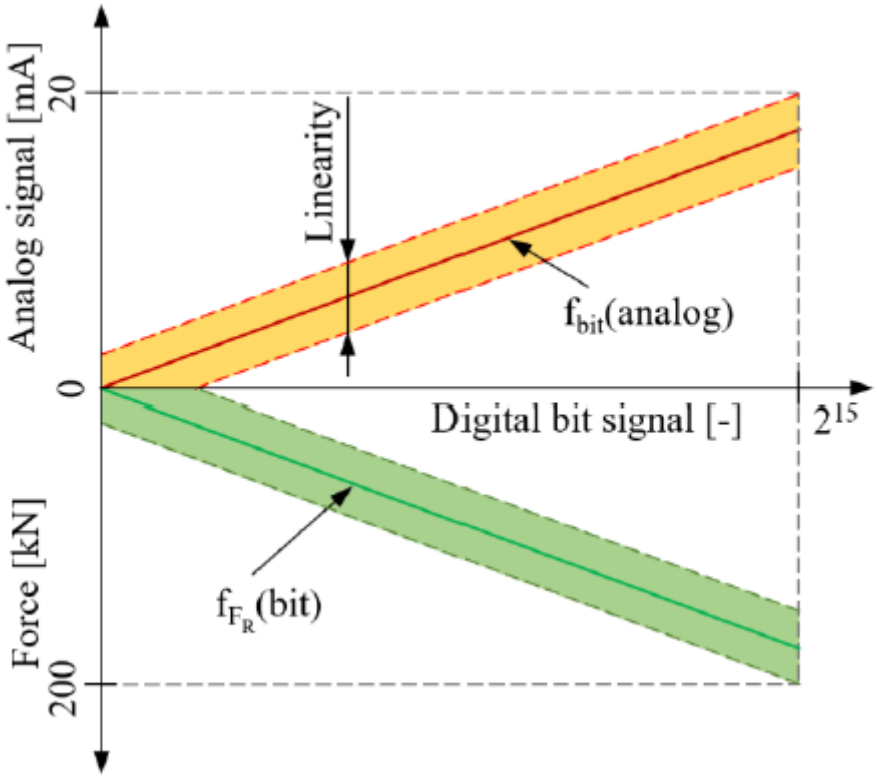

Figure 13

A/D input signal to physical quantity transformation: example rolling mill

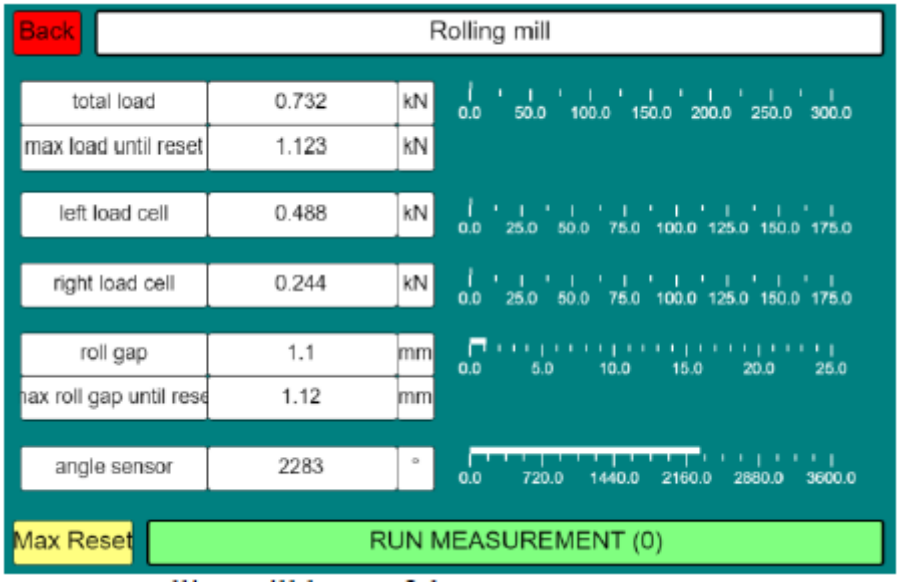

Figure 14

Rolling mill layer of the WAGO GUI

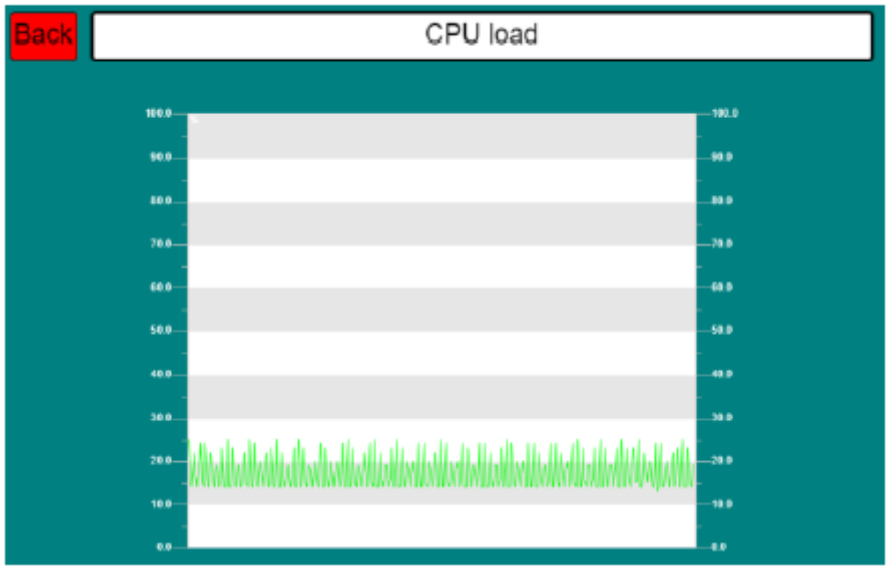

Figure 15

CPU load layer of Node 1: connected machines turned off

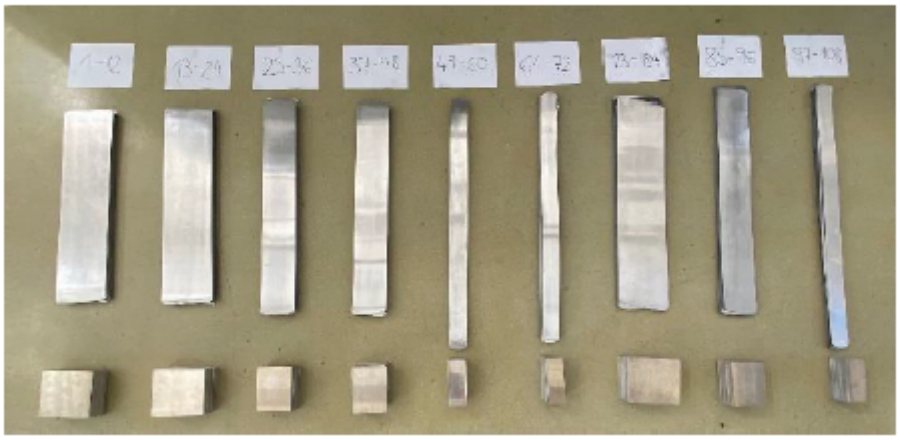

Figure 16

Processed sheet specimens: rolled (T1, top); initial (T2, bottom)

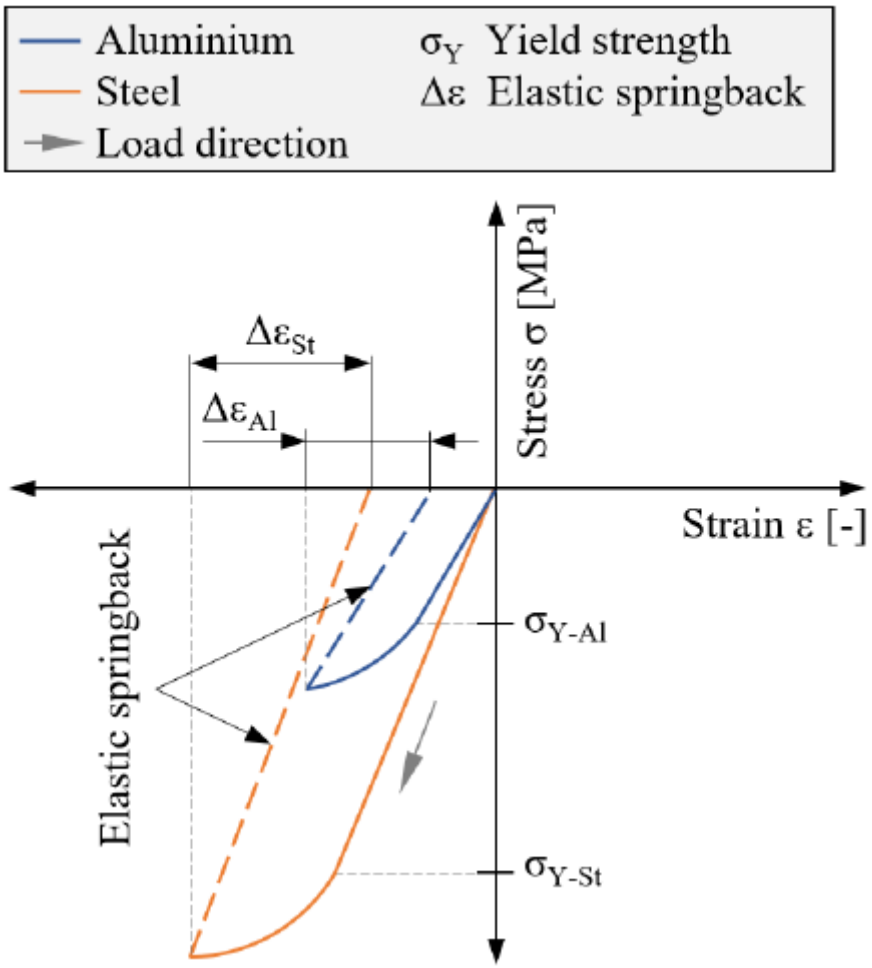

Figure 17

Elastic stiffness and corresponding effect on h1 during rolling

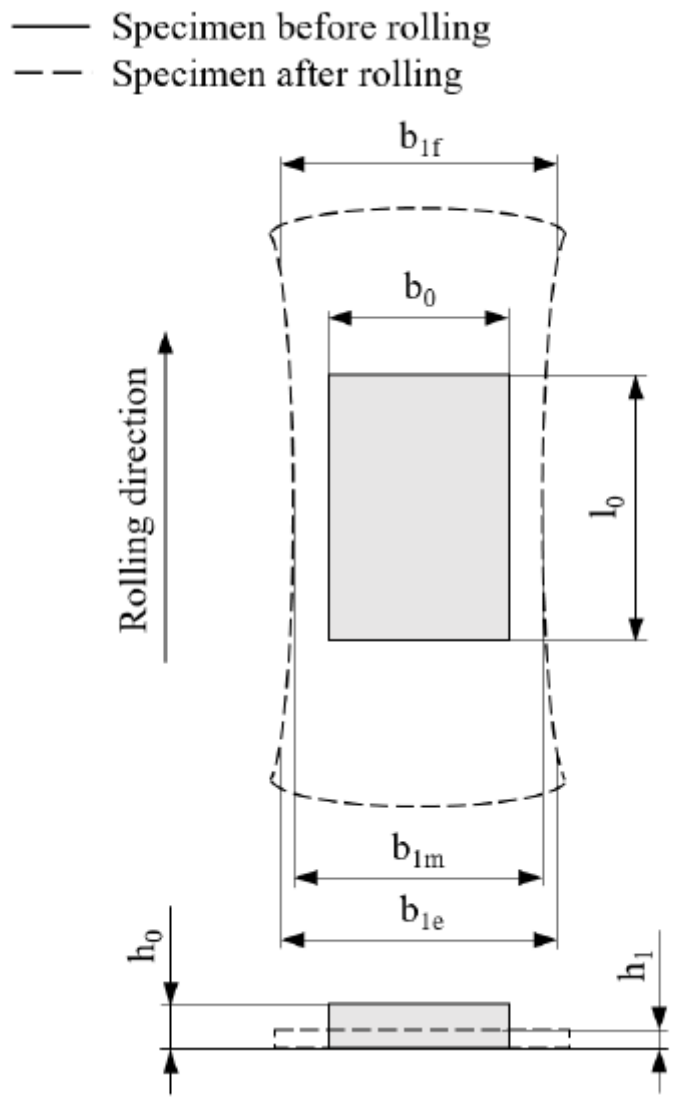

Figure 18

Sheet width measurement after rolling

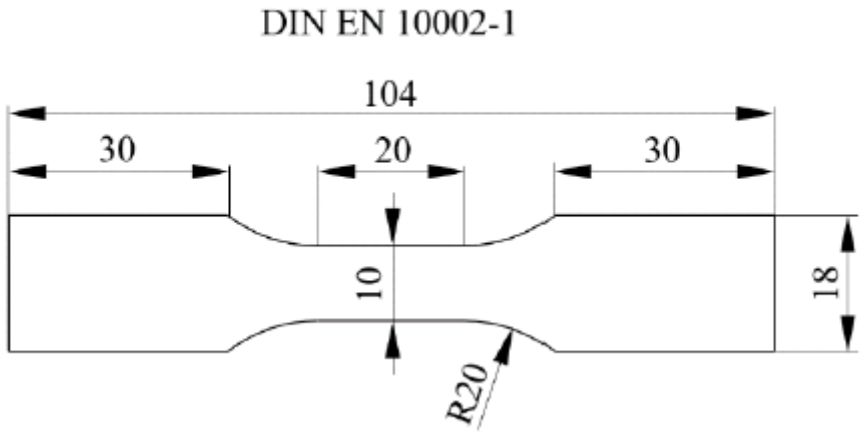

Figure 19

Tensile test: initial geometry (German Institute for Standardization)

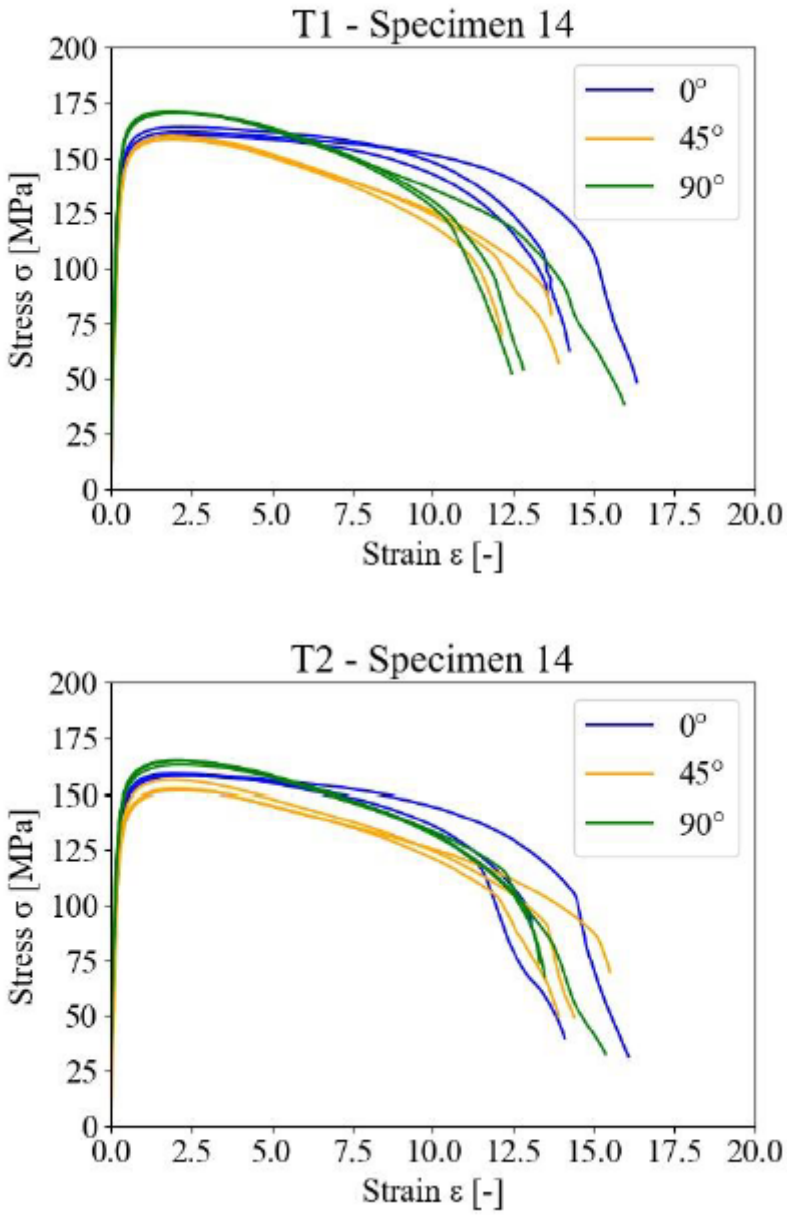

Figure 20

Specimen nr. 14: mechanical anisotropy T1/T2

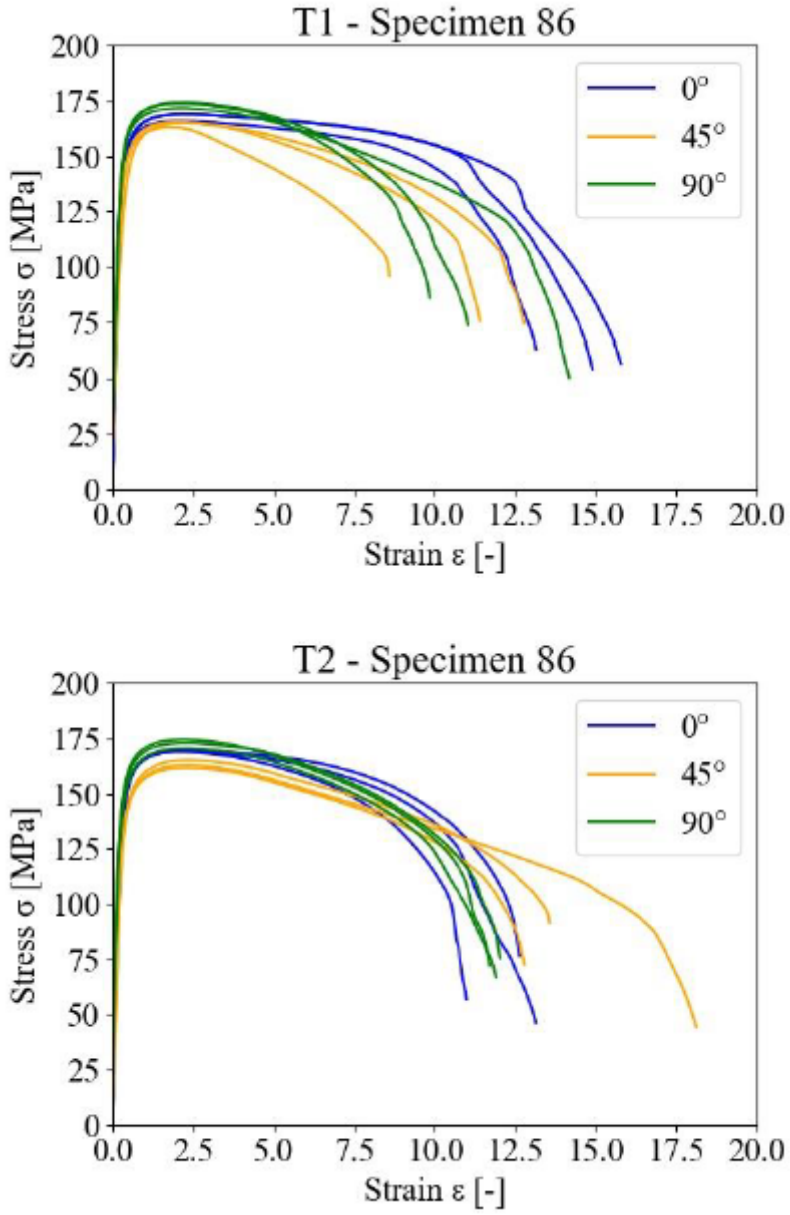

Figure 21

Specimen nr. 86: mechanical anisotropy T1/T2

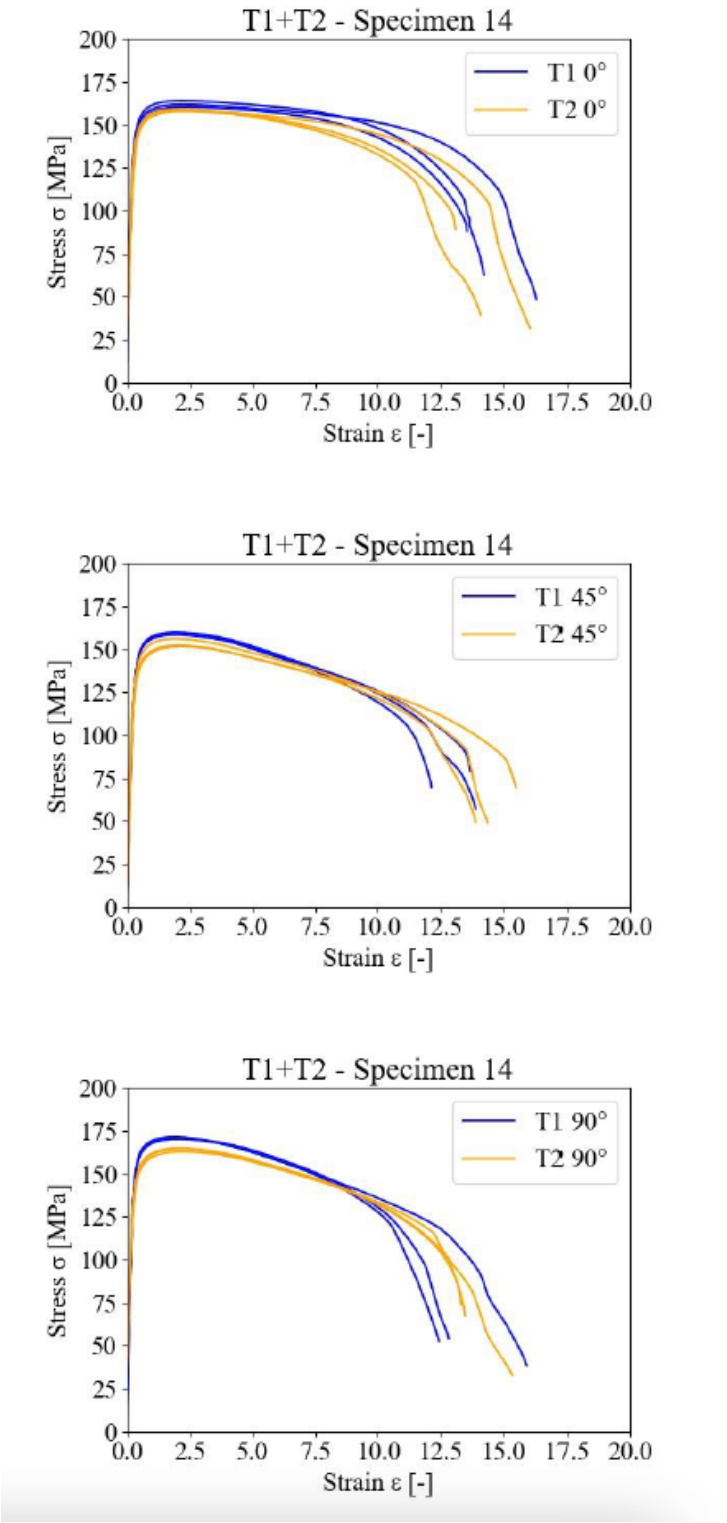

Figure 22

Direct comparison: specimen nr. 14

Figure 23

Direct comparison: specimen nr. 86

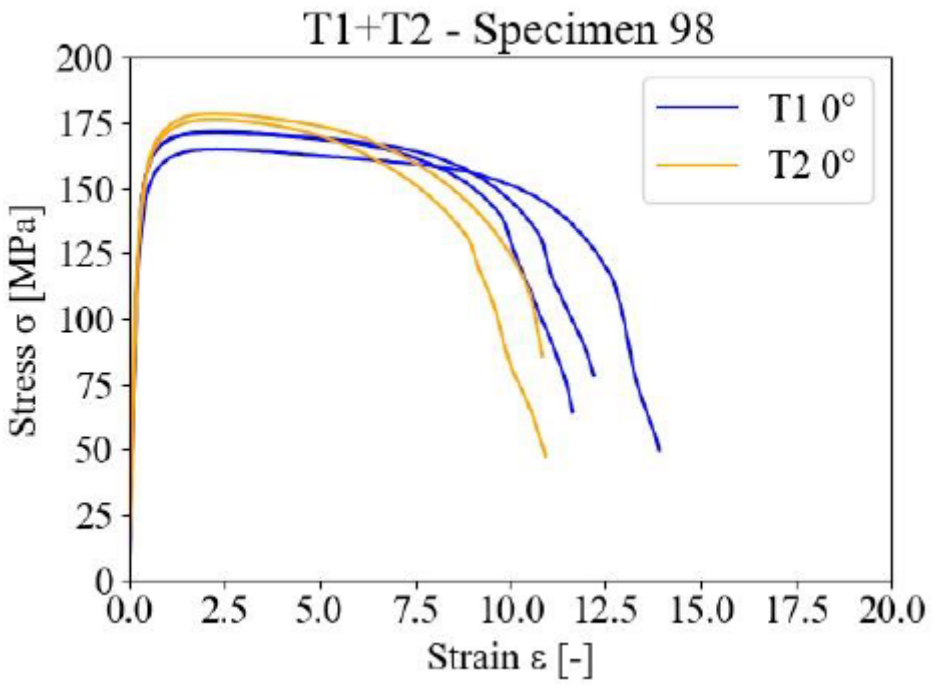

Figure 24

Direct comparison: specimen nr. 98

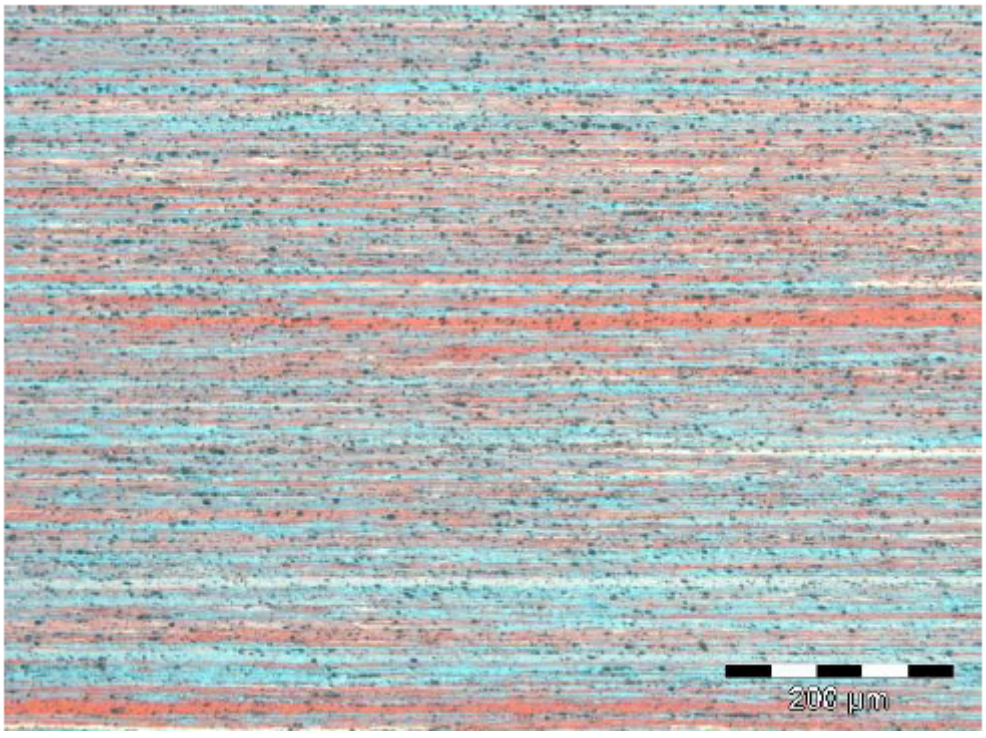

Figure 25

Exemplary OMI: initial microstructure in rolling direction (T1 /specimen nr. 86, 0°)

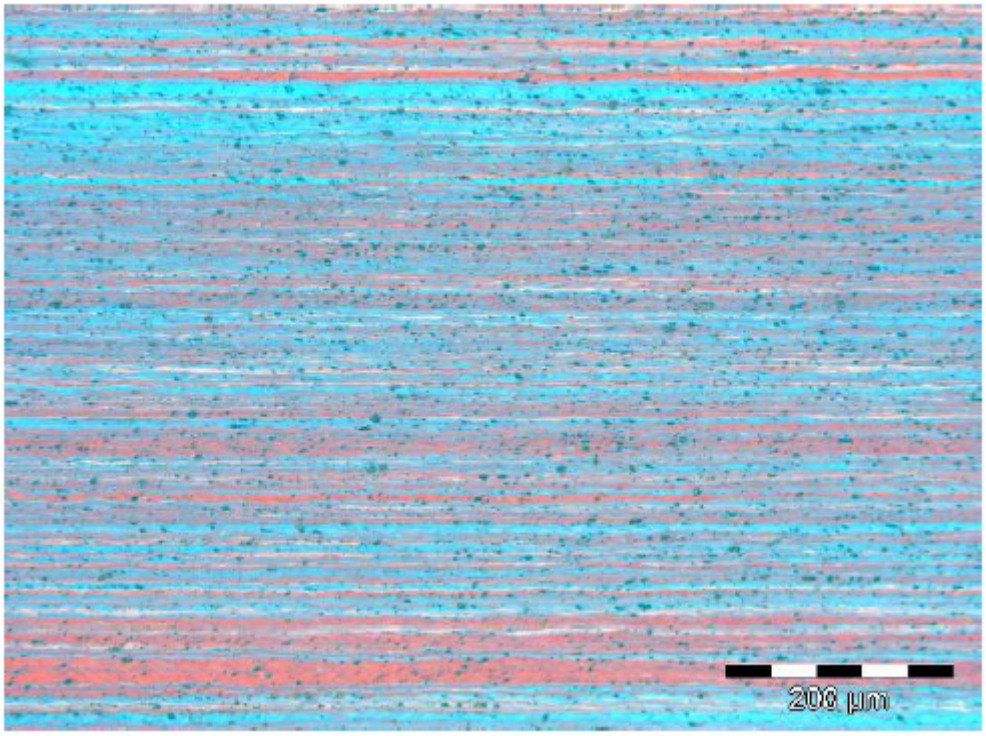

Figure 26

Exemplary OMI: microstructure after the rolling process (T1 /specimen nr. 86, 0°)

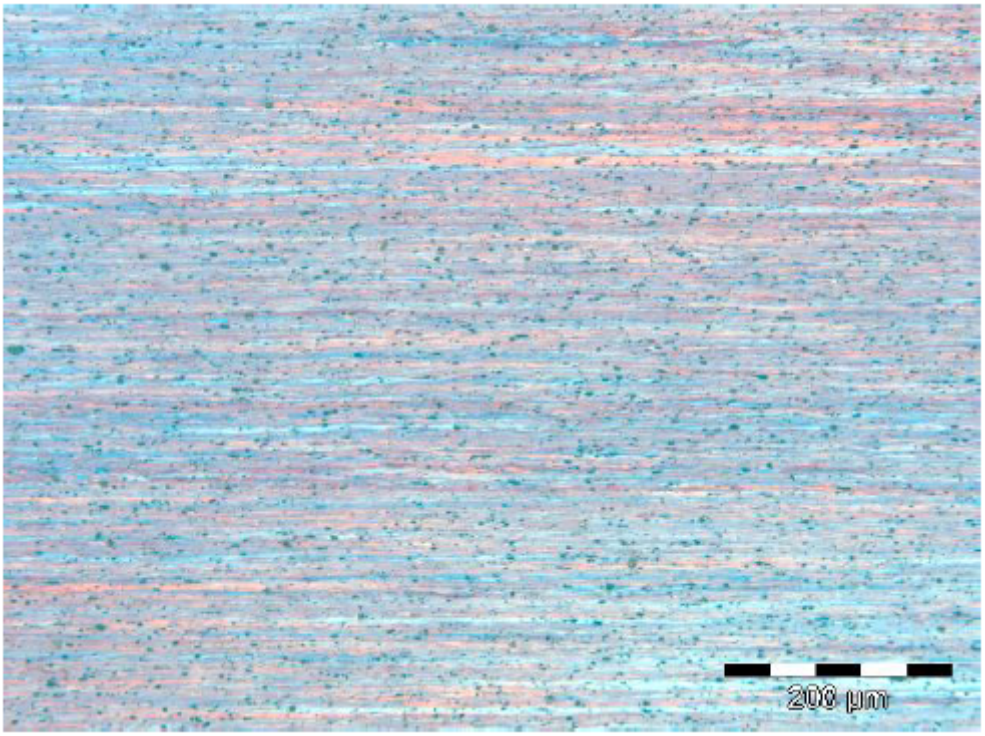

Figure 27

Exemplary OMI: microstructure after the rolling process (T1 /specimen nr. 86, 45°)

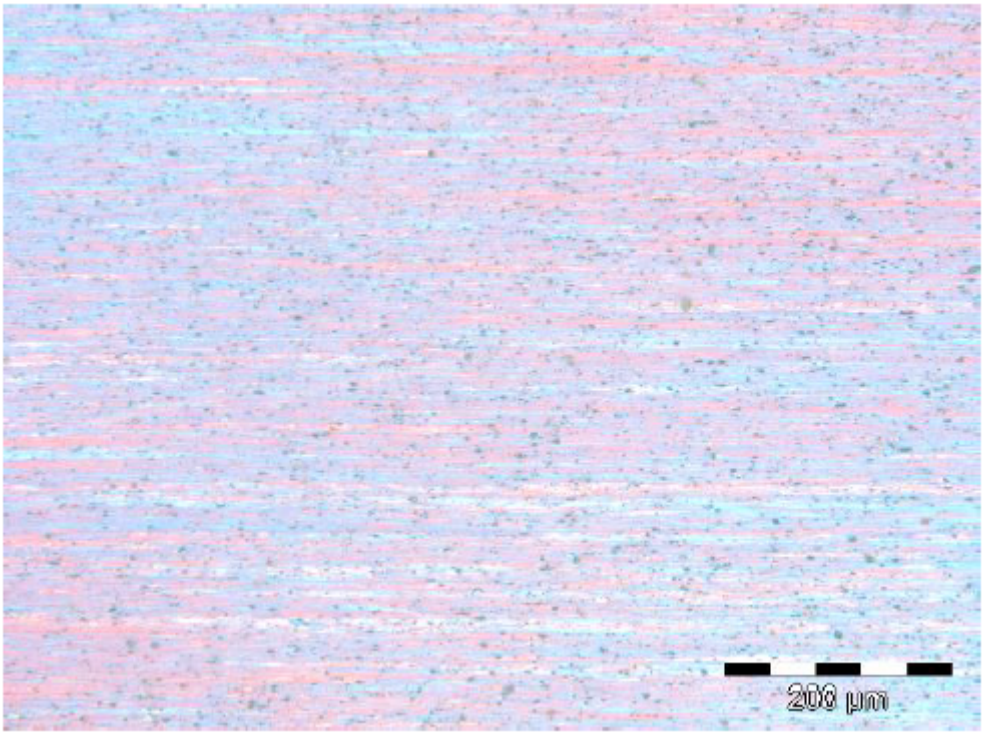

Figure 28

Exemplary OMI: microstructure after the rolling process (T1 /specimen nr. 86, 90°)

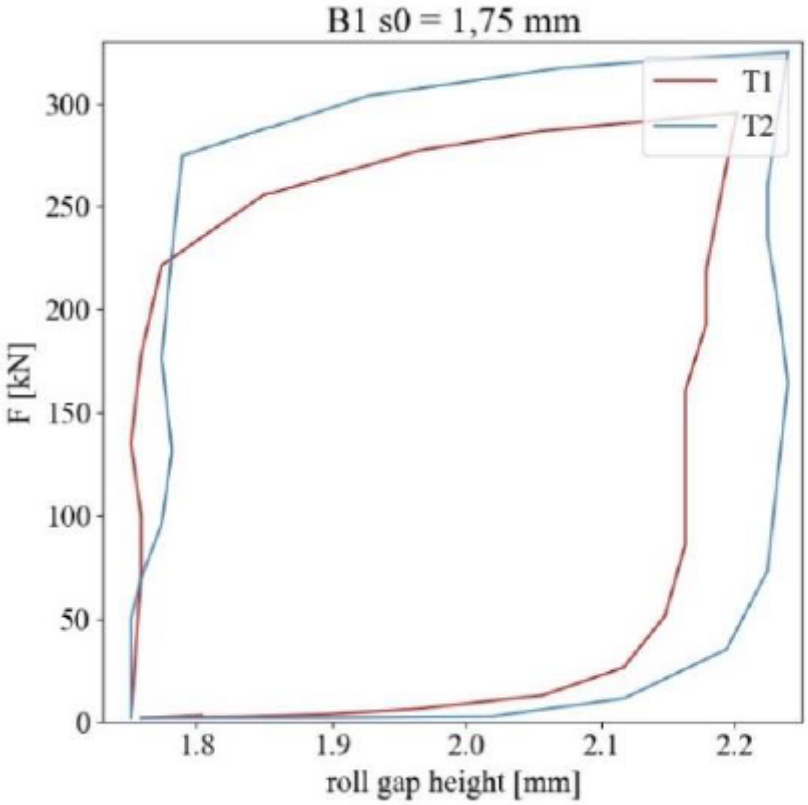

Figure 29

Example of a rolling hysteresis: B1 for s0 = 1.75mm

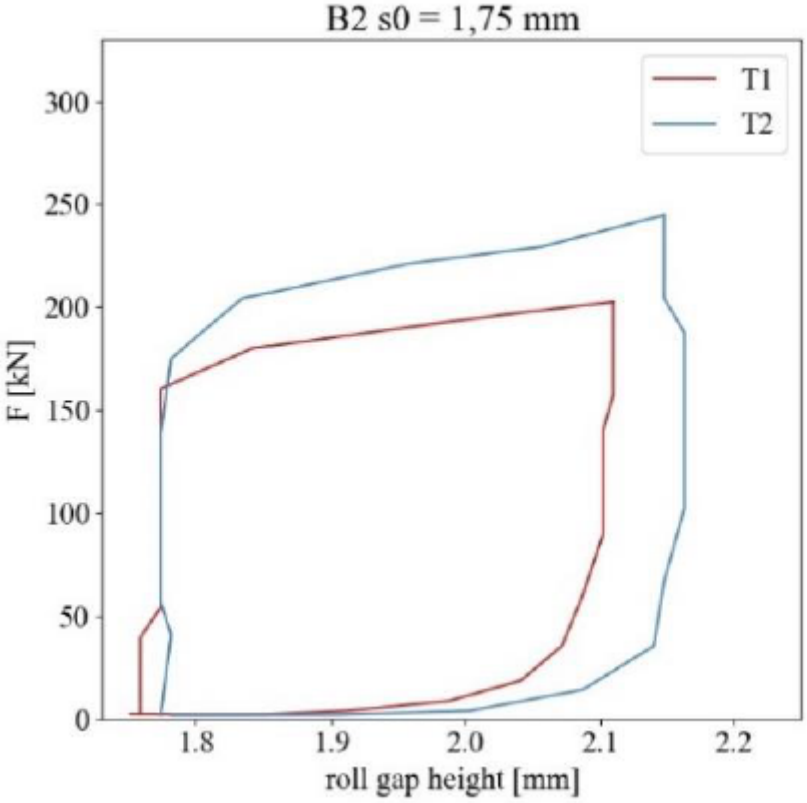

Figure 30

Example of a rolling hysteresis: B2 for s0 = 1.75mm

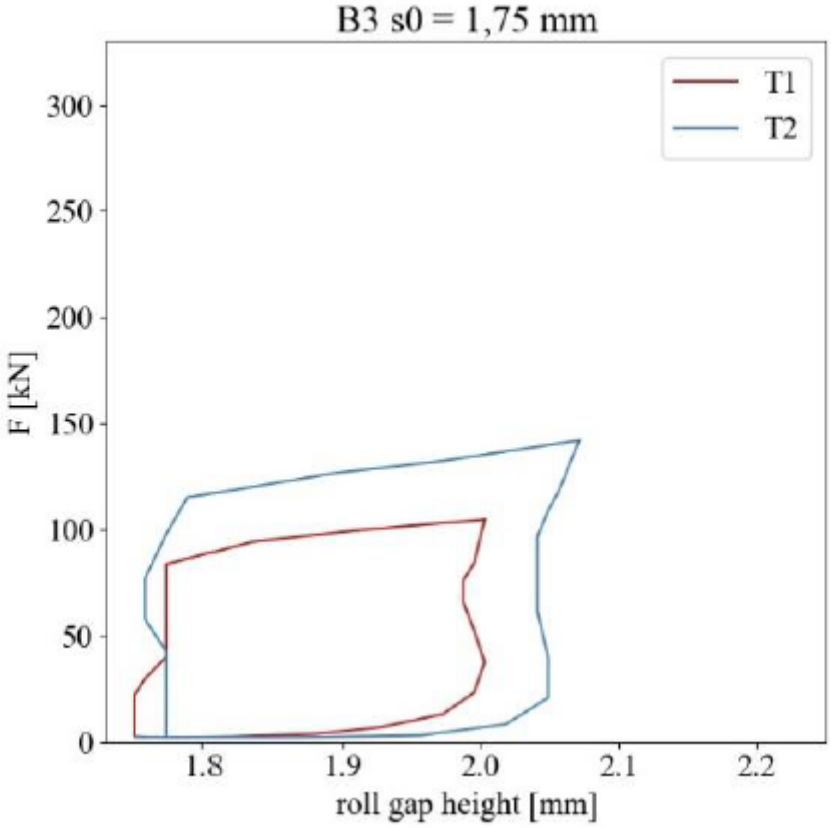

Figure 31

Example of a rolling hysteresis: B3 for s0 = 1.75mm

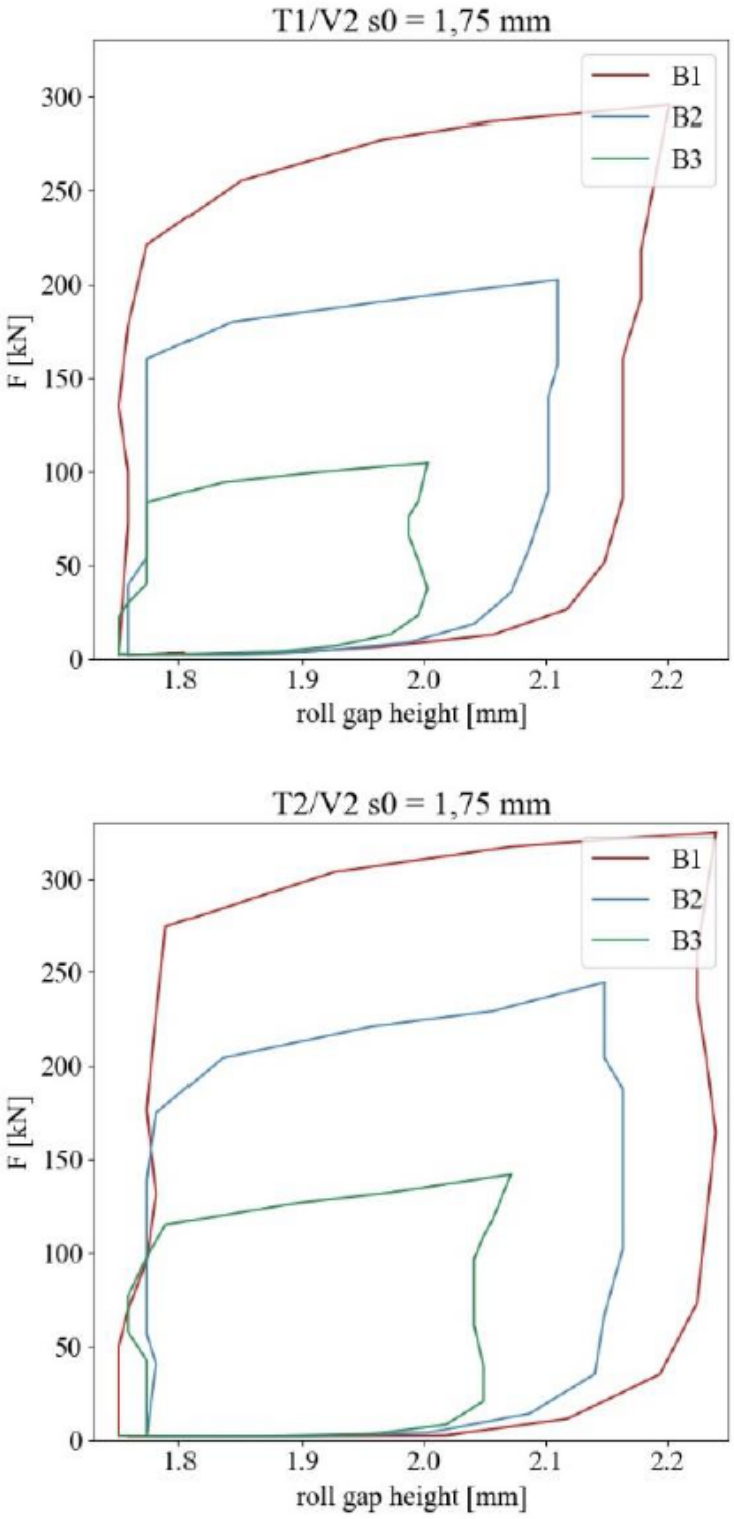

Figure 32

Rolling hysteresis: resulting FR as a function of initial sheet width: comparison between T1 (top) and T2 (bottom)

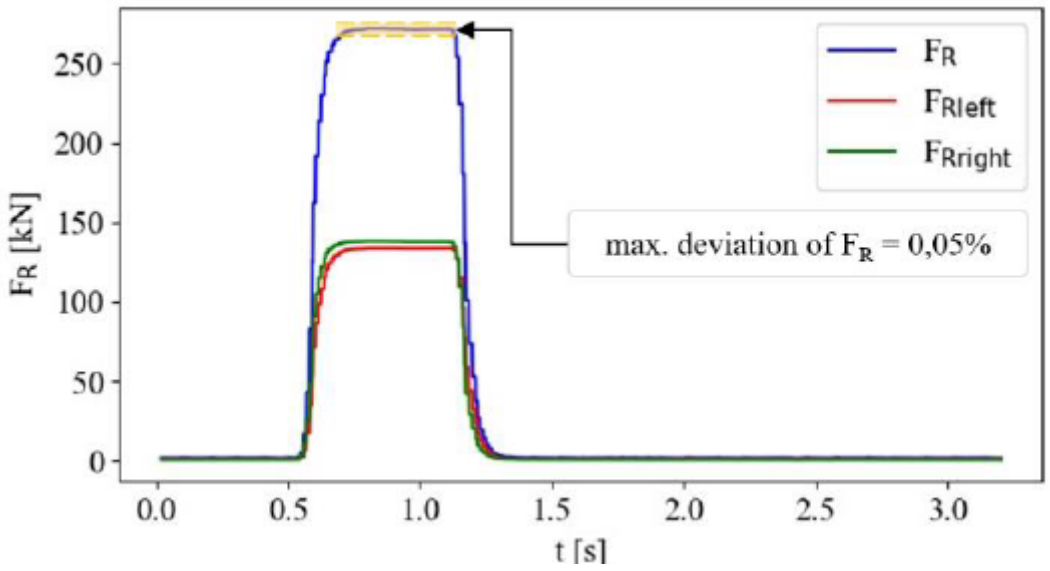

Figure 33

Exemplary rolling force-time curve

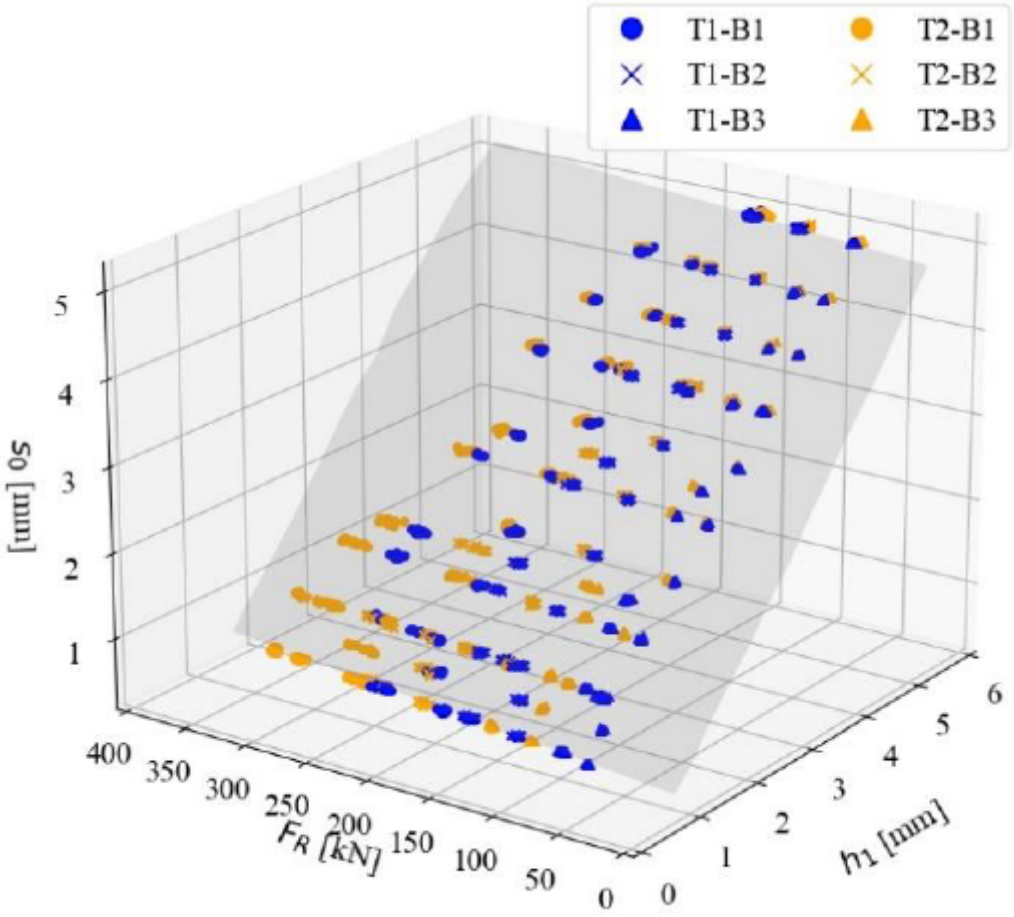

Figure 34

Resulting data points (1736) from the test and calibration data series

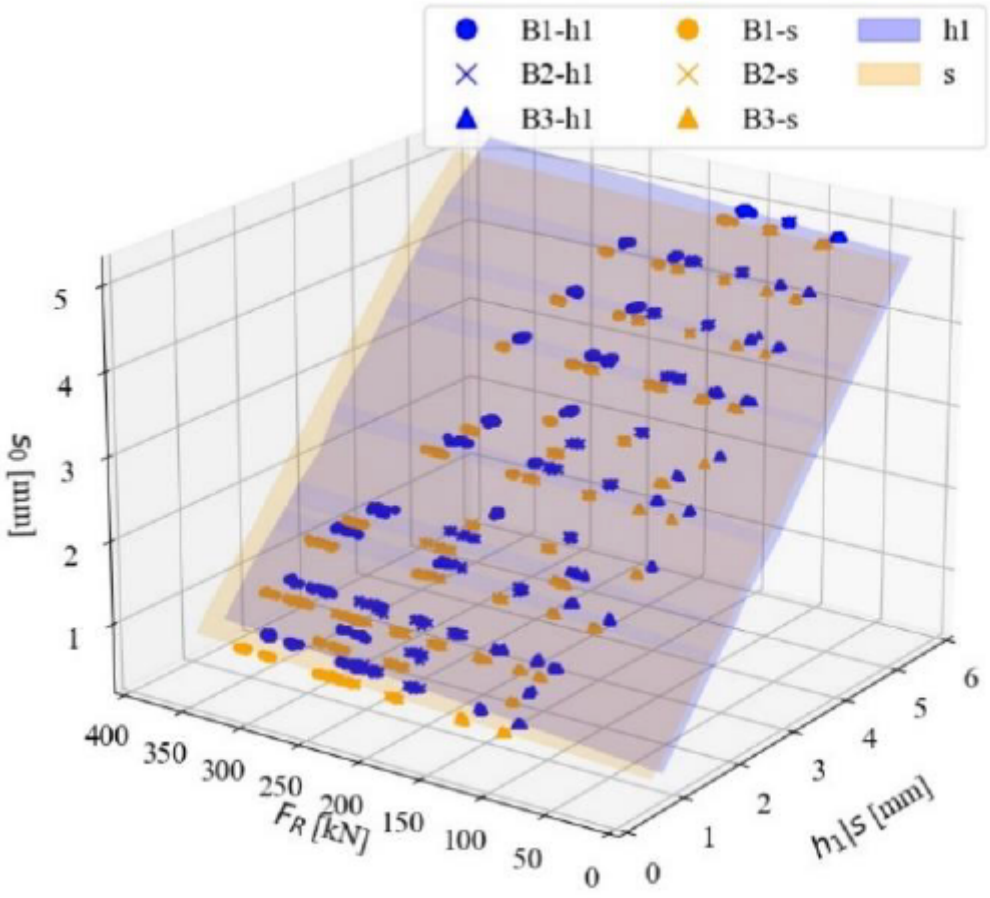

Figure 35

Comparison between resulting s (yellow plane) and h1 (blue plane) for B1, B2 and B3 within test series T1

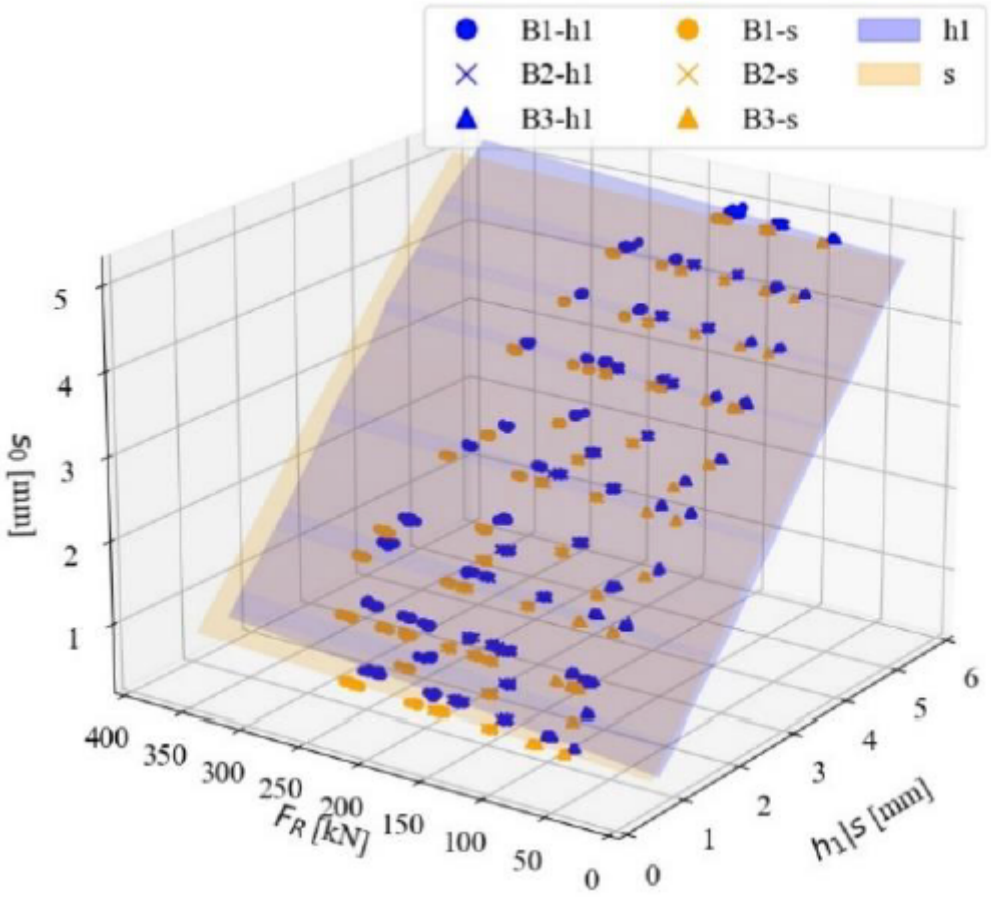

Figure 36

Comparison between resulting s (yellow plane) and h1 (blue plane) for B1, B2 and B3 within test series T2

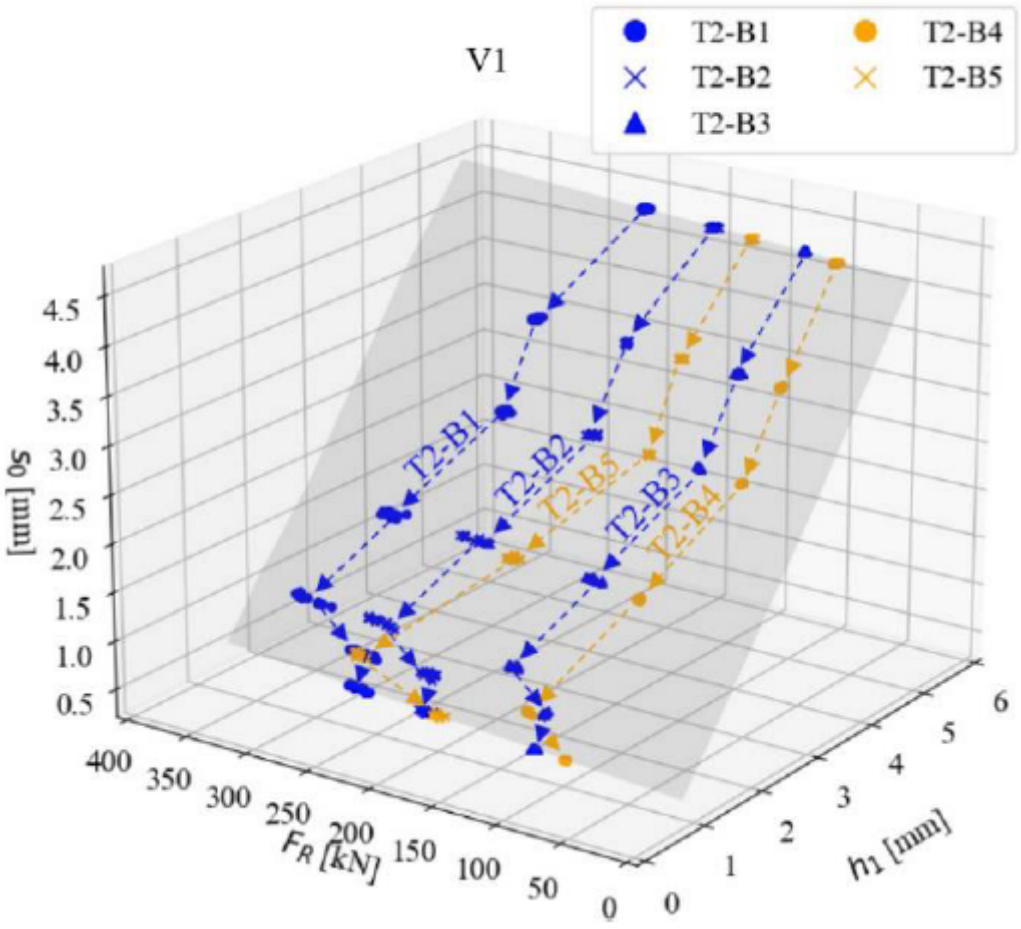

Figure 37

Implementation of validation data: comparison with V1 of test and calibration data sets

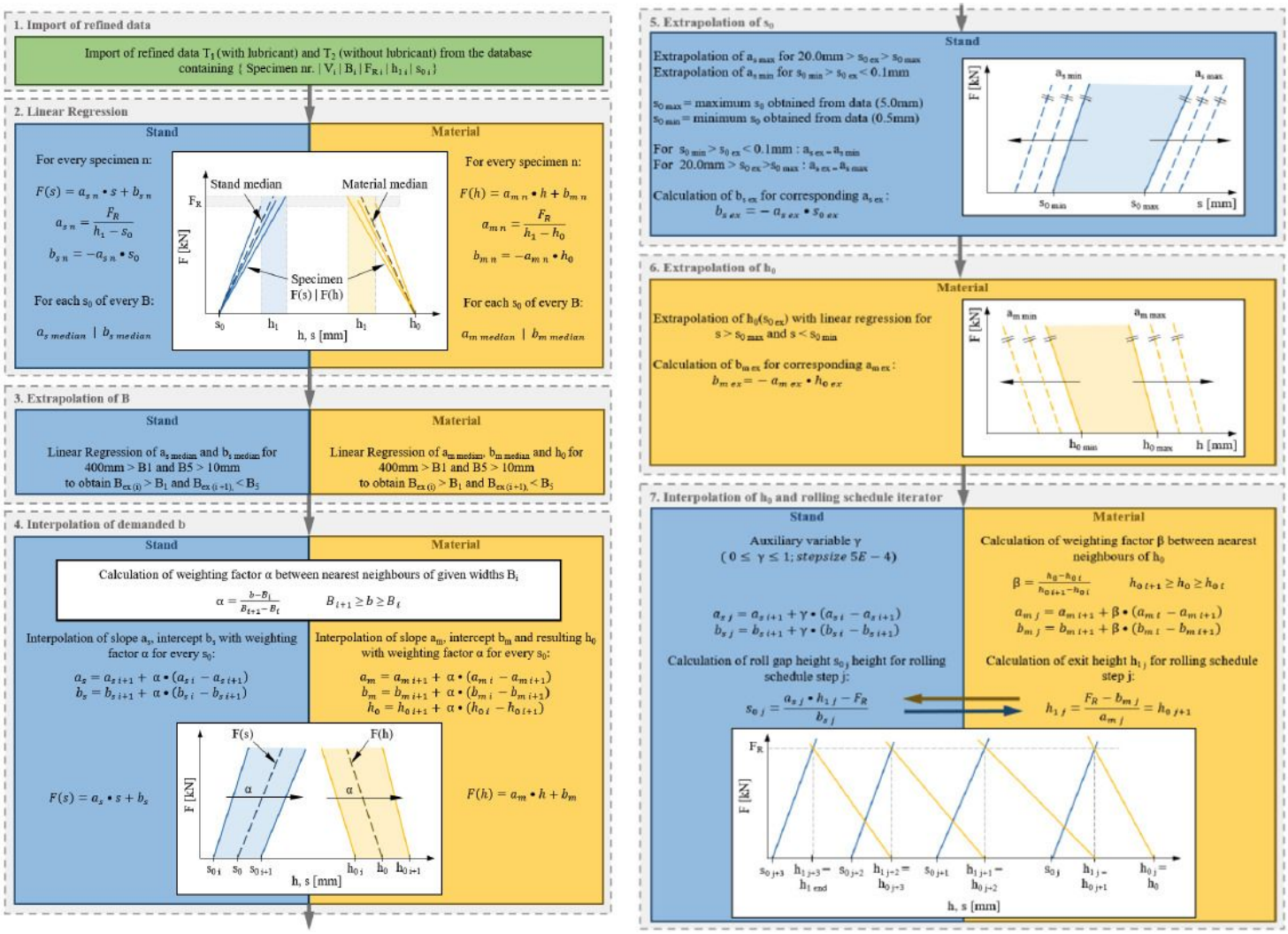

Figure 38

Fundamental logic for the Python based rolling schedule iterator

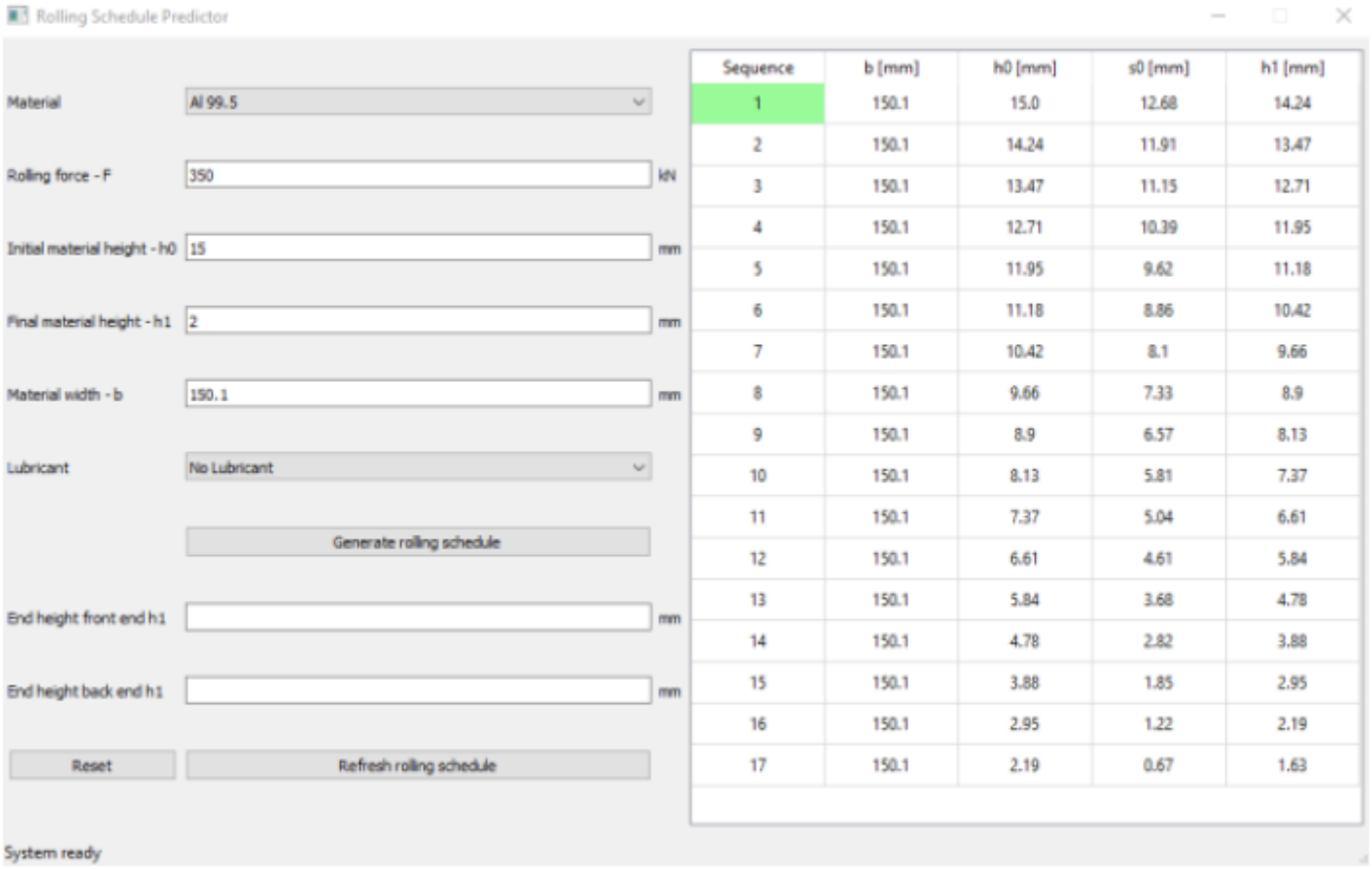

Figure 39

Resulting front end GUI for the rolling scheme iterator

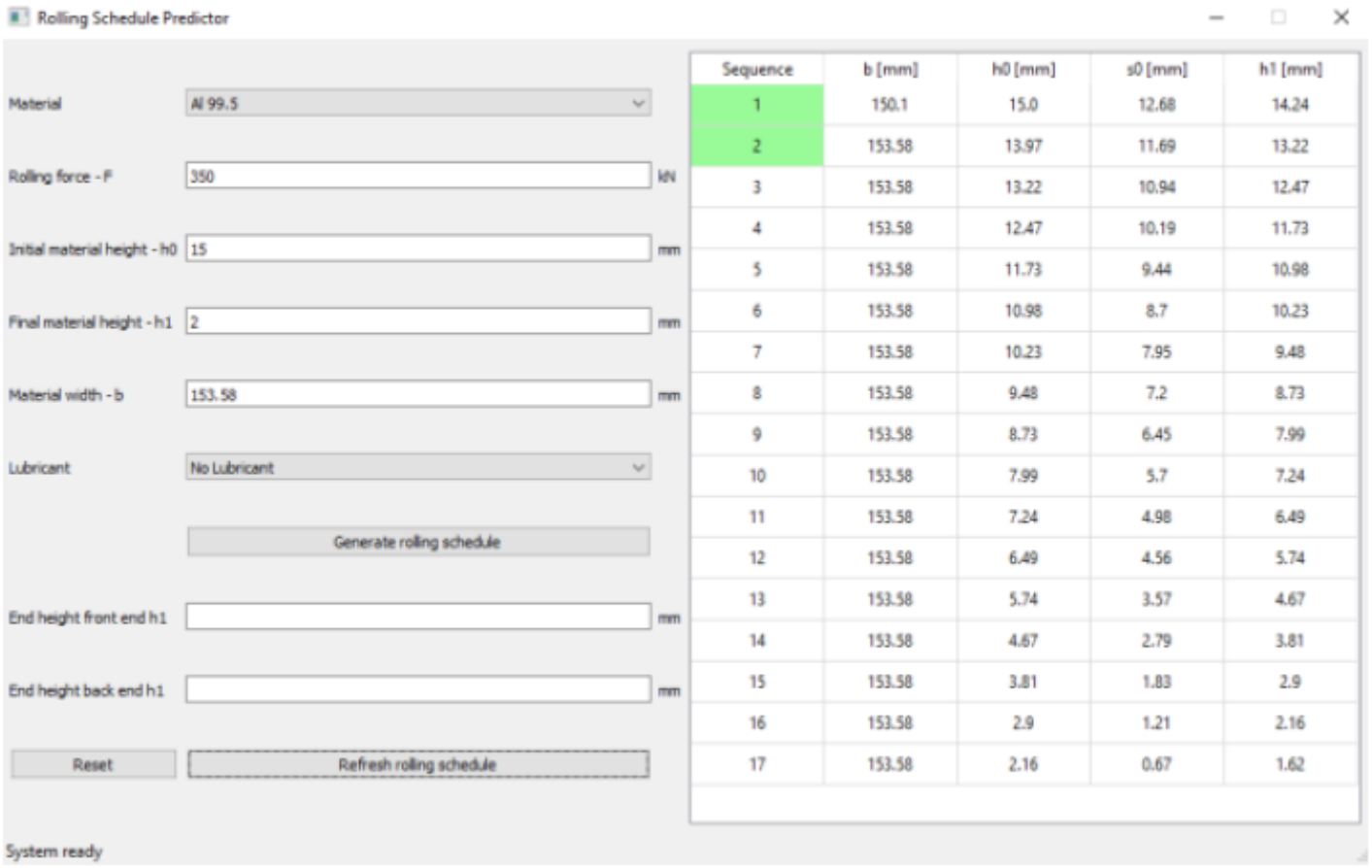

Figure 40

Changed parameters based on fig. 38 after the first rolling step: increased width and deviation between measured and predicted h1

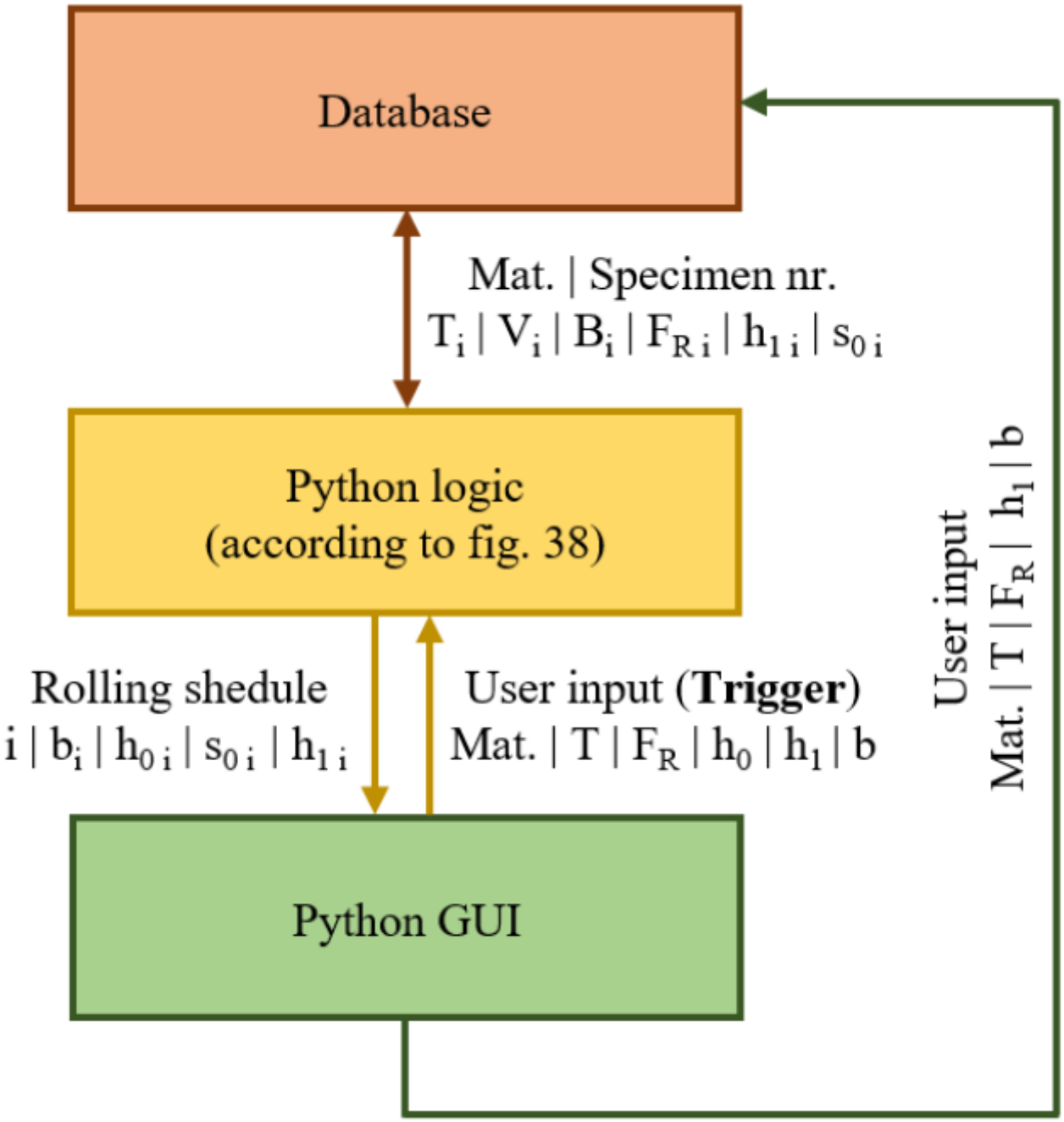

Figure 41

Overview of the interaction between the database, the corresponding logic (back-end GUI) and visualization (front-end GUI)

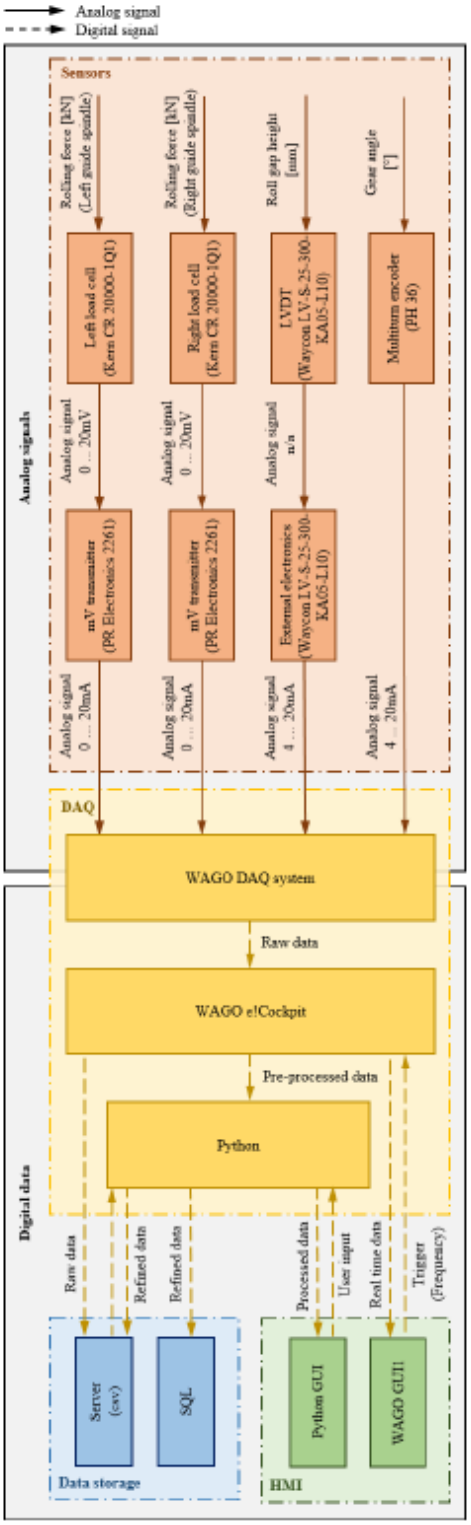

Figure 42

Resulting data flow for the digitalized rolling mill

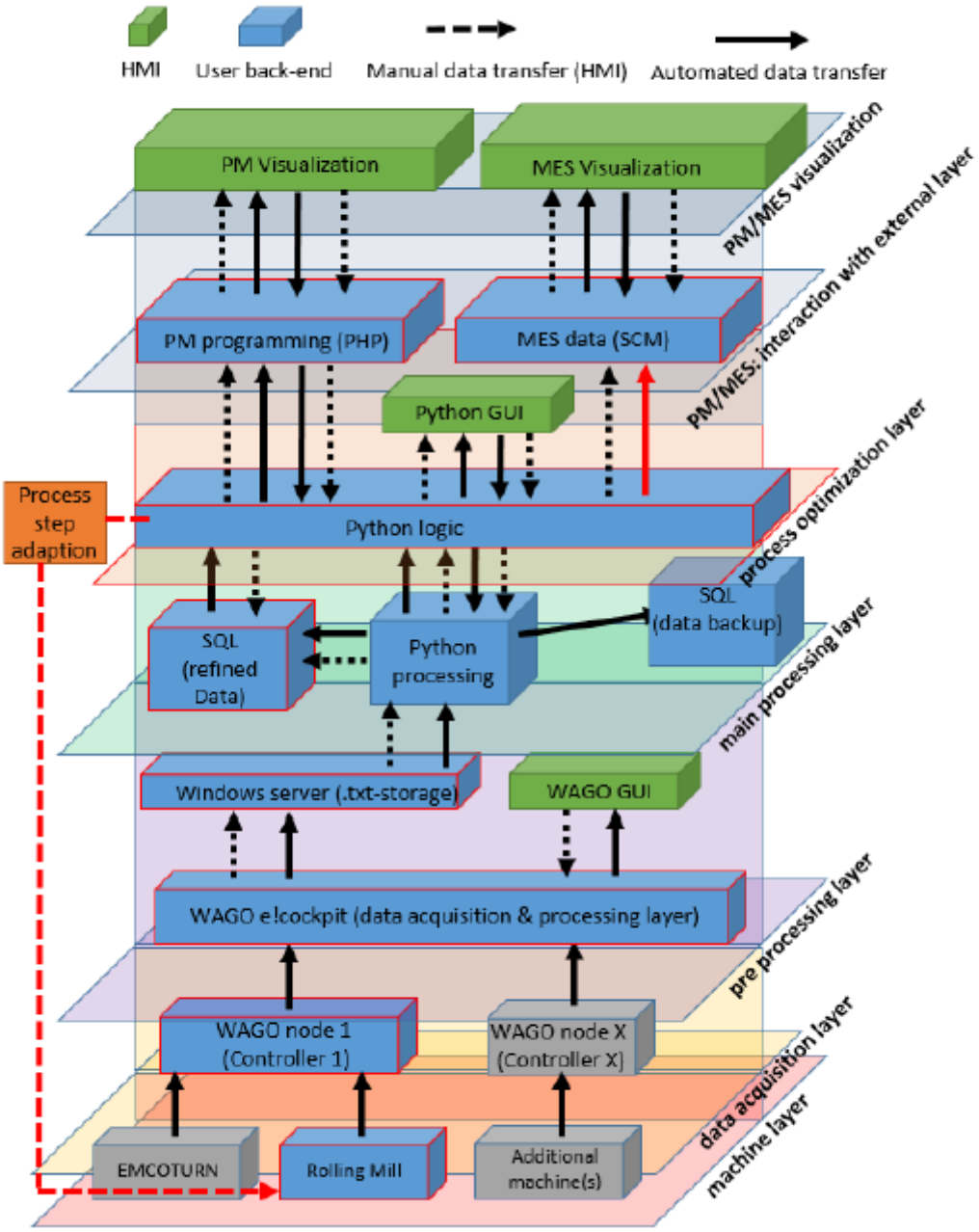

Figure 43

Resulting layer architecture for the developed CPPS